Posttranscriptional Regulation of the Human LDL Receptor by the U2-Spliceosome

Paolo Zanoni, Grigorios Panteloglou, Alaa Othman, Joël T. Haas, Roger Meier, Antoine Rimbert, Marta Futema, Yara Abou Khalil, Simon Flyvbjerg Norrelykke, Andrzej Jerzy Rzepiela, et al.

HAL Id: hal-03554168
https://hal.science/hal-03554168

Submitted on 22 Mar 2022

Posttranscriptional regulation of the human LDL Receptor by the U2-spliceosome

Paolo Zanoni[1,2,*], Grigorios Panteloglou[1,2,*], Alaa Othman[3], Joel T. Haas[4], Roger Meier[5], Antoine Rimbert[6], Marta Futema[7], Yara Abou Khalil[8,9], Simon F. Norrelykke[5], Andrzej J. Rzepiela[5], Szymon Stoma[5], Michael Stebler[5], Freerk van Dijk[10], Melinde Wijers[6], Justina C. Wolters[6], Nawar Dalila[11], Nicolette C. A. Huijkman[6], Marieke Smit[6], Antonio Gallo[12], Valérie Carreau[12], Anne Philippi[13], Jean-Pierre Rabès[8,14,15], Catherine Boileau[8,16], Michele Visentin[17], Luisa Vonghia[18,19], Jonas Weyler[18,19], Sven Francque[18,19], An Verrijken[19,20], Ann Verhaegen[19,20], Luc Van Gaal[19,20], Adriaan van der Graaf[10], Belle V. van Rosmalen[21], Jerome Robert[1], Srividya Velagapudi[1,2], Mustafa Yalcinkaya[1,2], Michaela Keel[1,2], Silvija Radosavljevic[1,2], Andreas Geier[22], Anne Tybjaerg-Hansen[11], Mathilde Varret[8], Lucia Rohrer[1,2], Steve E. Humphries[23], Bart Staels[4], Bart van de Sluis[6], Jan Albert Kuivenhoven[6], and Arnold von Eckardstein[#,1,2]

* These authors contributed equally to this work

Author affiliations:

1. Institute for Clinical Chemistry, University and University Hospital Zurich, Zurich, 8091 Switzerland.
2. Center for Integrative Human Physiology, University of Zurich, Zurich, 8057 Switzerland.
3. Institute of Molecular Systems Biology, ETH Zurich, 8093, Zurich, Switzerland.
4. University of Lille, Inserm, CHU Lille, Institut Pasteur de Lille, U1011- EGID, 59000 Lille, France.
5. Scientific center for optical and electron microscopy (ScopeM), ETH Zurich, 8093, Zurich, Switzerland.
6. Department of Pediatrics, Section Molecular Genetics, University of Groningen, University Medical Center Groningen, 9713 AV Groningen, the Netherlands.
7. Cardiology Research Centre, Molecular and Clinical Sciences Research Institute, St George's, University of London, London, UK.
8. LVTS-INSERM UMRS 1148 and University of Paris, CHU Xavier Bichat, 75018, Paris, France.
9. Laboratory of Biochemistry and Molecular Therapeutics (LBTM), Faculty of Pharmacy and Pôle technologie Santé (PTS), Saint-Joseph University, 1104 2020, Beirut, Lebanon.
10. University of Groningen, University Medical Center Groningen, Department of Genetics, 9713AV, Groningen, The Netherlands
11. Department of Clinical Biochemistry, Rigshospitalet, Copenhagen University Hospital, Faculty of Health and Medical Sciences, University of Copenhagen, 2100 Copenhagen, Denmark.
12. AP-HP, Endocrinology and Metabolism Department, Human Research Nutrition Center, Pitié-Salpêtrière Hospital, 75013 Paris, France.
13. Université de Paris, Faculté de Médecine Paris-Diderot, UMR-S958, Paris, France. Current address: Université de Paris, Institut Cochin, INSERM U1016, CNRS UMR-8104, Paris, France.
14. AP-HP, Université Paris-Saclay, 75004, Paris, France.
15. UFR Simone Veil des Sciences de la Santé, UVSQ, 78180 Montigny-Le-Bretonneux, France.
16. AP-HP, Genetics Department, CHU Xavier Bichat, Université de Paris,75018 Paris, France.
17. Department of Clinical Pharmacology and Toxicology, University Hospital Zurich, 8091, Zürich, Switzerland
18. Department of Gastroenterology and Hepatology, Antwerp University Hospital, 2650 Antwerp, Belgium.

19. Laboratory of Experimental Medicine and Paediatrics, Faculty of Medicine, University of Antwerp, 2610 Antwerp, Belgium.
20. Department of Endocrinology, Diabetology and Metabolism, Antwerp University Hospital, 2650 Edegem, Belgium.
21. Department of Surgery, Academic Medical Center, University of Amsterdam, 1105 AZ, Amsterdam, The Netherlands
22. Division of Hepatology, Department of Medicine II, University Hospital Würzburg, 97080 Würzburg, Germany.
23. Cardiovascular Genetics, Institute of Cardiovascular Science, University College London, WC1E 6JJ London, United Kingdom.

Actual affiliations at the moment of submission

- P.Z. is affiliated to the Institute of Medical Genetics, University of Zürich, 8952 Schlieren, Switzerland

- A.R. is affiliated to Inserm UMR 1087 / CNRS UMR 6291 IRS-UN, 44007, Nantes, France

- M.Y. is affiliated to the Division of Molecular Medicine, Department of Medicine, Columbia University, New York, 10032, NY, USA

- S.V. is affiliated to the Center for Molecular Cardiology, University of Zurich, 8952 Schlieren, Switzerland

Short title: U2 spliceosome regulates LDL receptor

Contact information:

Arnold von Eckardstein; Institute for Clinical Chemistry, University Hospital Zurich, Rämistrasse 100, 8091 Zurich, Switzerland; +41 44 255 22 60; arnold.voneckardstein@usz.ch

Word count: 7888 excluding title page and abstract

Keywords: LDL-cholesterol, LDL receptor, spliceosome, intron retention, RNA interference, genome wide screening

1 **Abstract**

2 *Background:* The low-density lipoprotein receptor (LDLR) in the liver is the major determinant of
3 LDL-cholesterol levels in human plasma. The discovery of genes that regulate the activity of LDLR
4 helps to identify pathomechanisms of hypercholesterolemia and novel therapeutic targets against
5 atherosclerotic cardiovascular disease.

6 *Methods* We performed a genome-wide RNA interference screen for genes limiting the uptake of
7 fluorescent LDL into Huh-7 hepatocarcinoma cells. Top hit genes were validated by in vitro
8 experiments as well as analyses of datasets on gene expression and variants in human populations.

9 *Results:* The knockdown of 54 genes significantly inhibited LDL uptake. Fifteen of them encode for
10 components or interactors of the U2-spliceosome. Knocking down any one of 11 out of 15 genes
11 resulted in the selective retention of intron 3 of *LDLR*. The translated LDLR fragment lacks 88% of
12 the full length LDLR and is detectable neither in non-transfected cells nor in human plasma. The
13 hepatic expression of the intron 3 retention transcript is increased in non-alcoholic fatty liver disease
14 as well as after bariatric surgery. Its expression in blood cells correlates with LDL-cholesterol and age.
15 Single nucleotide polymorphisms and three rare variants of one spliceosome gene, *RBM25,* are
16 associated with LDL-cholesterol in the population and familial hypercholesterolemia, respectively.
17 Compared to overexpression of wild type *RBM25*, overexpression of the three rare *RBM25* mutants in
18 Huh-7 cells led to lower LDL uptake.

19 *Conclusions:* We identified a novel mechanism of post-transcriptional regulation of LDLR activity in
20 humans and associations of genetic variants of *RBM25* with LDL-cholesterol levels.

21

1   **Introduction**

2   Hypercholesterolemia is a causal and treatable risk factor of atherosclerotic cardiovascular
3   diseases (ASCVD)[1]. The most important determinant of LDL-cholesterol (LDL-C) levels in plasma is
4   the hepatic removal of circulating LDL by binding to the LDL receptor (LDLR) for subsequent
5   endocytosis and degradation[2]. The expression of LDLR is tightly regulated by transcription factors,
6   proteasomal and lysosomal degradation, endosomal recycling, and cleavage at the cell surface[1,2]. The
7   unravelling of this complex regulation led to the development of drugs that effectively lower plasma
8   levels of cholesterol and, as the consequence, risk of ASCVD[1].

9   To identify novel regulators of LDL uptake into the liver, we performed an image-based genome-wide
10 RNA interference (RNAi) screen in Huh-7 human hepatocarcinoma cells. Fifteen out of 54 genes
11 significantly reducing LDL uptake upon knockdown encode for proteins involved in pre-mRNA
12 splicing. The majority of them are either core components or interactors of the U2-spliceosome[3]. By
13 functionally validating this finding *in vitro* as well as in human tissues, we provide evidence that a
14 functional U2 spliceosome is needed for the expression of full length LDLR and, hence, determining
15 LDLR activity in humans.

16

1 **Methods**

2 **Data Availability**

3 The authors declare that all data and methods supporting the findings of this study are
4 available in the Data Supplement or from the corresponding authors on reasonable request.

5 A detailed description of materials and methods is provided in the text and Major Resources
6 Table of the Online Supplement

7

8 **Results**

9 **The U2-spliceosome and its interactors are rate-limiting for LDL endocytosis**

10 For the genome wide RNAi screen of genes limiting uptake of LDL or HDL, Huh-7 human
11 hepatocarcinoma cells were reverse-transfected using three different siRNA oligonucleotides against
12 each of the 21,584 different human genes. To control efficacy and specificity of transfection, each
13 plate contained wells with cells transfected with siRNAs against *PLK1* whose knockdown results in
14 cell death, and *LDLR,* respectively. Based on results of time and dose finding experiments, the cells
15 were exposed 72 hours post transfection to 33 µg/mL each of Atto594-labelled LDL and Atto655-
16 HDL for 4 hours. As background controls, wells with cells transfected with a non-targeting siRNA
17 were incubated in the absence of fluorescent lipoproteins. After washing, fixation, and staining of the
18 nuclei with Hoechst 33258, the plates were imaged at 4x and 20x with two twin wide-field automated
19 microscopes. Nuclei, the relative cytoplasm, and fluorescent LDL-containing vesicles were identified
20 through automated image analysis (Figure 1A). Transfection efficiency was very high (Figure S1a).
21 Analysis and validation of HDL image data will be subject of a separate report.

22 For the uptake of fluorescent LDL, the five best performing assay features (foci count per cell, foci
23 mean intensity, cytoplasm granularity 1 and 2, cytoplasm median intensity) showed a high degree of
24 correlation. Therefore and because of the widest dynamic range based on Z'-factor values from control
25 wells, we identified gene hits by the Redundant siRNA Activity (RSA) analysis of data from the
26 median cytoplasm intensity feature. Z'-factor values for median cytoplasm intensity in each assay
27 plate for both the background (median 0.00, interquartile range [IQR] -023 to 0.20) and positive
28 control (median -0.56, IQR -0.99 to -0.20) clustered mostly around the 0-line, indicating a suboptimal
29 but analytically exploitable signal-to-noise ratio (Figure S1b). Dimensionality reduction of main assay
30 features did not significantly alter the outcome (Figures S1c and S1d). At an RSA p value cut-off of p
31 $< 10^{-3}$, interference with 54 and 37 genes decreased and increased LDL uptake, respectively (Table 1,
32 Table S1). By contrast to the findings of a previous genome wide CRISPR-based screening in Huh7
33 cells[4], our list does not include *LDLR* or its modulators such as *SCAP*, *MBTPS1*, or *IDOL/MYLIP*
34 except *AP2M1*, which is an essential contributor to clathrin-mediated endocytosis (Table 1). Gene
35 Ontology (GO) enrichment analysis showed significant clustering for genes whose loss of function
36 decreased LDL uptake (Table S2). Functional clustering of these genes with the STRING tool
37 revealed four major groups: the ribosome (N = 7), the proteasome (N = 8), the spliceosome (N = 15),
38 and vesicular transport (N = 5) (Figure 1B). Out of the 15 spliceosome genes, six encode for core
39 components of the U2 spliceosome, namely *SF3A1*, *SF3A2*, *SF3B1*, *SF3B2*, *SF3B5* and *SF3B6*. Other
40 proteins, interact with the U2-spliceosome either directly (AQR, ISY1 and RBM25) or indirectly
41 (RBM22)[3].

42 To confirm the role of the U2 spliceosome in LDL endocytosis *in vitro*, we performed ^{125}I-LDL cell
43 association assays in Huh-7 and HepG2 cells. *SF3B4* was also included in these experiments as it is
44 part of the U2 spliceosome and barely missed the RSA p value cut-off (p = 1.4*10^{-3}). Knockdown was
45 achieved using 4 pooled siRNA molecules against each hit gene acquired from vendors other than that
46 of the siRNA screening library, namely Dharmacon or Sigma instead of Ambion. (see Major Resource
47 Table and figure S2a). For *RBM25* we replaced Dharmacon's siRNAs with those from Sigma because
48 of their presumable off-target effects on LDLR protein expression (Figure S3). Knockdown of each of
49 these genes significantly decreased the specific cell association of ^{125}I-LDL with both Huh-7 and
50 HepG2 cells (Figures 1C,1D and Figure S2b). The association of ^{125}I-LDL was equally decreased by
51 knockdown of *SF3B1* (-45±5%), *SF3A2* (-47±6%), *AQR* (-45±6%), and *LDLR* (-43±8%) (Figure 1C).

1   RNA interference with *RBM25* reduced the specific cellular association of ^{125}I-LDL and fluorescent
2   LDL by 27% ±8% and 52%±5%, respectively (Figure 1D and Figure S3f). Of note, the specific cell
3   association of ^{125}I-HDL was unaltered or even increased upon knockdown of *AQR* and *SF3A1* in either
4   Huh-7 or HepG2 cells (Figures S2c and S2d).

5

**6   Loss of U2-spliceosome genes and their interactors causes selective retention of *LDLR* intron 3
7   (IVS3)**

8   To unravel the mechanism through which the U2-spliceosome and its interactors regulate LDL
9   endocytosis, we applied RNA sequencing to Huh-7 cells, which were transfected with either siRNAs
10   against eleven U2-spliceosome genes or a non-targeting control siRNA. Sequences can be accessed by
11   codes PRJEB46899 and PRJEB46898 in the data bank of the European Nucleotide Archive
12   (https://www.ebi.ac.uk/ena/browser/support) 72 hours after transfection, we measured both expression
13   at the gene level and alternative exon usage in polyA-selected transcripts. Knockdown of all eleven
14   genes except *RBM25* induced a marked increase in the retention of intron 3 of *LDLR* in mature
15   transcripts without altering the expression of the *LDLR* full length transcript (Figure 2A, Figure S4).
16   This effect was confirmed in Huh-7 cells by qRT-PCR upon knockdown of *AQR*, *SF3B1, or RBM25*
17   by employing a primer set that was previously used to study the effects of the rare LDLR c.313+1,
18   G>A intronic variant, which leads to *LDLR* loss of function by constitutively promoting intron 3
19   retention[5] (Figure S5a). By contrast to the RNA sequencing (Figure S4), qRT-PCR unravelled
20   increased expression of the *LDLR* IVS3 retention transcript upon knockdown of *RBM25*, albeit not as
21   much as with knockdown of *SF3B1* and *AQR* (Figures S5b and S5c).

22   Among all intronic or exonic sequences in the transcriptome, the expression of the intron 3
23   retaining *LDLR* transcript was altered most strongly. Upon knockdown of *SF3B1*, *AQR, or SF3A2*, the
24   retained intronic sequence of *LDLR* ranked at the top of each respective dataset when the exon-level
25   expression data was plotted against each other (Figure 2B). The degree of intron 3 retention upon
26   knocking down U2-spliceosome genes was significantly correlated with the decrease in ^{125}I-LDL cell
27   association, (r = -0.73, p = $1.4*10^{-2}$, Figure 2C).

28   To investigate reasons for intron 3 retention in *LDLR*, we transfected HEK293T cells with two
29   minigenes containing different portions of the *LDLR* genomic sequence flanked by two artificial exons
30   (Figure 3A). The first minigene (MG_1) encoding only for exon 3 of *LDLR* and the adjacent intronic
31   regions cloned between two artificial exons (SD6 and SA2), displayed very low if any RNA
32   sequencing reads mapping to the first ~130bp of intron 3. On the contrary, upon expression of the
33   whole genomic sequence between the 3'-end of intron 2 and the 5'-end of intron 4 of *LDLR* (MG_2) an
34   increased number of reads mapped to the first section of intron 3. This indicates incomplete splicing of
35   intron 3 when the physiological exon 4 acceptor site and the branch point site (BPS) were present in
36   the larger minigene MG_2 (Figure 3B). The acceptor splice site of exon 4 of *LDLR* hence appears to be
37   poorly defined. The bioinformatic analysis of the portion of intron 3 neighbouring exon 4 by the U2
38   branchpoint prediction algorithm SVM-BP-finder
39   (http://regulatorygenomics.upf.edu/Software/SVM_BP/)[6] identified one plausible U2-spliceosome
40   dependent BPS located 30 bp upstream of the acceptor site (Table S3). The *gtgat* pentamer in the
41   centre of the *cggtgatgg* branchpoint sequence was associated with very low U2 binding energy and
42   occurs at low frequency in the branchpoint database[6]. We discarded another predicted branchpoint 124
43   bp upstream of the acceptor site as the subsequent AG-exclusion zone does not reach up to the
44   acceptor. Contrary to exon 4 of human *LDLR*, exon 4 of murine *Ldlr* contains a strong and frequently
45   recurring branchpoint 33 bp upstream of the acceptor site (Figure 3C). This finding is in accordance
46   with intron 3 of *Ldlr* being barely detectable at the RNA level by qRT-PCR in mouse liver (data not
47   shown). Taken together, these data suggest that the BPS of intron 3 in human *LDLR* is poorly defined
48   and therefore very sensitive to alternative splicing.

49

50   Selective intron 3 retention limits LDLR cell surface abundance

51   The transcript with intron 3 retention encodes for a prematurely truncated proteoform of
52   LDLR because the 5'-end of intron 3 encodes for 12 novel amino acids followed by a stop codon.

1   Including the signal peptide, this theoretical 116 amino acid residues long and 12.7 kDa large
2   'LDLRret fragment' encompasses the complete first and large part of the second class A domains
3   (labelled as L1 and L2 in Figure 4A[7]) but lacks all other domains, including the transmembrane
4   portion of LDLR. Western blots probed with an antibody against the C-terminus of LDLR revealed
5   60±30% and 61±13% lower LDLR protein levels upon knockdown of *AQR* and *SF3B1*, respectively
6   *(*Figures 4B and 4C). A similar decrease in LDLR protein was seen upon knockdown of *RBM25* with
7   siRNAs from Sigma (-68%±10%), whereas the knockdown of *RBM25* with the siRNA of Dharmacon
8   led to an increase in LDLR protein (+122%±109%), presumably due to off target effects (Figures S3d
9   and S3e). Flow cytometry experiments on alive Huh-7 cells after *SF3B1* and *AQR* knockdown showed
10   a -87%±1% and –61%±4%, respectively, lower cell surface abundance of LDLR (Figure 4D). The
11   knockdown of *RBM25* with siRNAs from Sigma and Dharmacon decreased the cell surface abundance
12   of LDLR by 53%±6% and 21%±5%, respectively, as compared to non-targeting siRNAs from the
13   respective manufacturers (Figure S3g).

14   To investigate whether cells produce and secrete the LDLRret fragment, we overexpressed a
15   C-terminally HA-tagged version of the LDLRret fragment in HEK293T cells. 48 hours after
16   transfection, the HA-tagged LDLRret fragment was detectable in the cell lysates (Figure 4E) as well as
17   in undiluted cell culture media (Figure 4F). The proteasomal inhibitor MG-132 decreased cellular
18   LDLRret protein levels (Figure 4E) suggesting that the LDLRret fragment is not catabolized through
19   the proteasome. We also overexpressed an untagged version of the LDLRret fragment in HEK293T
20   cells. Targeted mass spectrometry recorded a peptide, which is present in both the full-length protein
21   and in LDLRret, over its basal endogenous level in HEK293T cell lysates (Figure S6) but not in
22   human plasma (data not shown).

23

A large proportion of *LDLR* transcripts in human liver and blood cells retains intron 3

25   To investigate its physiological or pathological relevance, we quantified *LDLR* intron 3
26   retention in liver biopsies as well as in peripheral blood cells by three different methods, and explored
27   associations with non-alcoholic fatty liver disease (NAFLD), demographic measures, lipid traits, and
28   therapeutic interventions.

29   qRT-PCR of mRNAs of liver tissue from 17 patients with benign liver tumours and 9 patients
30   with suspected NAFLD, found the *LDLR* intron 3 retention transcript expressed at considerable and
31   interindividually variable amounts (Figure 5A). Taking the sum of the full length and intron 3
32   retention transcripts of *LDLR* as the reference, 43 % (range 23% to 85%) of the transcripts retained
33   intron 3 (Figure 5A).

34   The bioinformatics analysis of RNA sequencing data on liver samples of 13 healthy non-obese
35   subjects, 12 obese subjects without NAFLD, 15 patients with NAFLD, and 15 patients with non-
36   alcoholic steatophepatitis (NASH) (Gene Expression Omnibus, accession number GSE126848)[8] found
37   14 different *LDLR* transcripts (Figure S7). Four transcripts showed the largest interindividual
38   variation, namely *LDLR-201* and *LDLR-208*, encoding full length *LDLR,* as well as *LDLR-206*, which
39   corresponds to the retained intron 3 transcript, and the likewise futile *LDR-214* (*LDLR* transcripts are
40   illustrated schematically in Figure S7a). Interestingly, the median concentration of *LDLR-206* was
41   substantially higher in patients with NAFLD or NASH than in normal weight or obese subjects
42   without NAFLD. The median percentages of *LDLR-206* reads relative to total reads from all
43   transcripts of *LDLR* gene increased significantly from 1.8% (range 0.7% to 4.2%) and 1.7% (0.4% to
44   3.7%) in normal weight and obese subjects without NAFLD, respectively, to 5.8% (1.1 to 26.7%) and
45   5.0% (0.9% to 29.0%) in patients with NAFLD and NASH, respectively (figure 5B). Of the two most
46   abundant full length encoding *LDLR* transcripts, *LDLR-208* decreased significantly (Figure 5C) while
47   the expression of *LDLR-201* did not change (Figure S7).

48   We also investigated the expression of *LDLR* transcripts in liver biopsies of 155 obese non-
49   diabetic subjects[9] by using Affymetrix Human Gene 2.0 ST arrays (see Table S4 for clinical and
50   biochemical characteristics). The signal intensities from a probe located in intron 3 of *LDLR* were
51   significantly higher than the other intronic *LDLR* probes located in introns 2, 4 and 15 and comparable
52   to probes located in coding exons (Figure 5D). The percent intensities of the IVS3 probe relative to the

1 sum of all *LDLR* probes ranged from 7.5% to 82%. Intron 3 retention correlated significantly only
2 with *SF3B1* (r =0.26, p=1.4*10^{-2}), while no U2-spliceosome gene showed any significant correlation
3 with overall *LDLR* expression (Table S5). Relative intensities of neither the intron 3 probe nor any
4 other of the 24 *LDLR* probes showed significant correlations with plasma levels of total, HDL- or
5 LDL-cholesterol (Figures S8a, S8b and S8c, Table S6). Correlations with histological NAFLD stages
6 were inverse by trend but not statistically significant (Figure S8d). Intron 3 relative probe intensity did
7 not correlate with BMI (Figure S8e) .However, in a subgroup of 21 patients who underwent a second
8 liver biopsy after bariatric surgery (median follow-up time = 13 months, IQR = [12, 15]), the
9 proportion of the intron 3 retention transcript relative to the full length *LDLR* transcript increased
10 significantly after surgery (p = 9.8*10^{-3}) (Figure S8f; Table S4). This increase was even more
11 pronounced in eleven patients with NASH at baseline but no NASH at follow-up (p = 3.6*10^{-2}, Figure
12 S8g).

13 Finally, we analyzed the RNA-sequencing data in whole blood samples from 2,462 subjects of
14 the Dutch BIOS consortium[10]. The *LDLR* ENST00000557958 transcript, predicted to retain intron 3,
15 was detectable in all subjects and represented 21%±7% of the total *LDLR* transcripts. The
16 ENST00000557958 transcript levels significantly correlated with age (r = 0.25, p = 9.2*10^{-36}, Figure
17 6A) and less strongly with LDL-C (r = 0.089, p = 3.9*10^{-5}, Figure 6B). The latter correlation lost its
18 statistical significance after adjusting for age, suggesting age itself as the main driver of the
19 association between ENST00000557958 levels and LDL-C. ENST00000252444, the only transcript
20 encoding for full length *LDLR* and expressed in blood cells in all subjects in this dataset, was also
21 positively correlated with age (r = 0.19, p = 8.8*10^{-20}, Figure 6C) but not with LDL-C (r = -0.033, p =
22 4.0*10^{-1}, Figure 6D). Correlation of neither transcript with BMI was statistically significant.

23

24 **Single Nucleotide Polymorphisms in *RBM25* are associated with lower LDL-Cholesterol**

25 The analysis of whole exome sequencing (WES) data of 40,468 UK Biobank subjects[11] did
26 not unravel any significant association between our spliceosome hit genes and LDL-C or any other
27 clinical lipid trait (Table S7). However, constraints data from the gnomAD database indicate a strong
28 intolerance to functional genetic variation for our U2-spliceosome genes, with a probability of
29 intolerance to loss of function (pLI)[12] of 0.91±0.17 (mean± SD) (Table S8). The analysis of SNPs of
30 11 U2-spliceosome hit genes in 361,194 participants of UK Biobank found 24 SNPs of *RBM25*
31 significantly associated with lower levels of LDL-C (Figure 7A) and apoB (Figure S9a).

32 In Europeans, four SNPs in introns or downstream of the *RBM25* coding sequence including
33 the lead SNP rs17570658 and two upstream SNPs are in almost complete LD (Figure S9b). , With R^2
34 > 0.8 no other SNP of RBM25 is in strong LD. A meta-analysis of eight studies with 455'537 samples
35 (https://cvd.hugeamp.org/variant.html?variant=rs17570658) and data of the Copenhagen City Heart
36 and General Population Studies[13] according to METAL[14] showed the association of rs17570658 with
37 LDL-C (Z Score = -4.181, p = 2.9*10^{-5}, Table S9).

38 *RBM25* is widely expressed in many tissues, but expression is relatively low in liver (GTeX
39 https://gtexportal.org/home/, data not shown). rs17570658 shows strong association with *RBM25*
40 expression in 15 different tissues including skeletal muscle and arteries (Figure 7B) as well as adipose
41 and mammary tissue, lung, oesophagus, kidney, and skin. Carriers of the rare allele have higher mean
42 *RBM25* mRNA concentration, which is compatible with higher LDLR activity and lower LDL-C
43 levels.

44

45 **Impaired LDL uptake by cells expressing rare *RBM25* mutants found in patients with**
46 **familial hypercholesterolemia**

47 In the UK10K study, *RBM25* was also among the genes identified to harbour an excess of rare
48 novel variants in 71 patients with familial hypercholesterolemia who are negative for mutations in
49 *LDLR*, *APOB* and *PCSK9*, the known FH-causing genes[15]. We re-analyzed the burden of variants in
50 the *RBM25* gene, using previously published WES data from 71 FH patients negative for mutations in
51 *LDLR*, *APOB* and *PCSK9*, and 56,352 European data provided by the gnomAD study[12]. Missense,

1   splice site, frameshift, and stop-gained variants identified by WES in both FH cases and gnomAD
2   were filtered to select those with MAF<$1.0*10^{-4}$. After filtering, three *RBM25* variants were found in
3   the FH cohort and 163 in the gnomAD Europeans cohort. (Table S10). Two variants, p.I152F
4   (c.454A>T) and p.A455D (c.1364C>A), were not found in any publicly available sequencing database
5   and hence appear unique to the FH cohort. The third variant, p.L17P (c.50T>C) (rs1167173761), was
6   found in one European individual in the gnomAD cohort (MAF = $9*10^{-6}$, allele count = 1/251402).
7   The comparison of variant numbers in FH cases vs. gnomAD using a binomial test demonstrated the
8   enrichment of rare variants in *RBM25* in the FH cohort (p = $1.0*10^{-3}$). Within the UK10K cohort, no
9   other U2-spliceosome gene was found to carry a rare presumable LOF mutation.

10   We investigated the functional consequences of overexpressing the three FH-associated RBM25
11   mutants in Huh-7 cells. Overexpression of all *RBM25* constructs was confirmed by qRT-PCR (Figures
12   S10a and S11a) and - for wild type RBM25 - Western blotting (Figure S10b). The overexpression of
13   neither wild type RBM25 nor any RBM25 mutant in Huh-7 cells caused significant changes in the
14   expression of full length or IVS3 retention transcripts of *LDLR* (Figures S10c, S10d, S11b, and S11c).
15   Compared to empty vector, overexpression of wild type RBM25 in Huh-7 cells changed neither the
16   cell surface abundance of LDLR nor LDL uptake significantly (Figures S10e and S10f). Comparisons
17   with cells overexpressing wild type RBM25 revealed minor decreases of LDLR cell surface levels
18   (Figure S11d) but more pronounced or even significant decreases of Atto655-LDL-uptake of cells
19   overexpressing the RBM25 mutants p.L17P (-15%±16%), I152F (-23%±12%), or p.A455D (-
20   28%±12%, p = $2.6*10^{-2}$) (Figure S11e).

21

22   **Discussion**

23   Through genome-wide siRNA screening, we discovered that the U2-spliceosome as well as
24   some interacting proteins, control LDLR levels and LDL uptake in liver cells by modulating the
25   selective retention of intron 3 of *LDLR*. The intron 3 retaining *LDLR* transcript encodes a truncated
26   and most probably non-functional receptor. In several cohorts of healthy individuals and patients, we
27   observed considerable interindividual variation of *LDLR's* IVS3 retention in liver as well as in
28   peripheral blood cells. Finally, we obtained initial evidence that rare genetic variants as well as SNPs
29   associated with its expression levels in the U2-spliceosome-associated gene *RBM25* are related to
30   LDL-C levels in humans. Taken together, our findings suggest intron 3 retention of *LDLR* as a novel
31   mechanism regulating LDLR activity and thereby plasma levels of LDL-C.

32   A previous siRNA screen also found U2-spliceosome genes to limit the uptake of LDL into
33   EA.hy926 cells but the authors excluded them from further analysis and validation[16]. Basic cellular
34   functionality of spliceosome genes may be the reason why U2- spliceosome genes were not found by a
35   previous CRISPR-based screen as limiting factors for LDL uptake into Huh-7 cells[4]. As these authors
36   discussed, CRISPR-based screens may overlook genes that are essential or confer a fitness advantage
37   in culture, since guide RNAs targeting those genes will be progressively depleted from the pooled
38   population[4].

39   As a preliminary mechanistic explanation, our minigene data as well as our *in silico*
40   predictions suggest that the BPS in intron 3 of human *LDLR* is poorly defined and thereby highly
41   sensitive to alterations in the activity of U2 splice factors. In this regard it is noteworthy that the rare
42   c.313+1, G>A intronic variant leads to loss of LDLR function by constitutively promoting IVS3
43   retention[5].

44   Medina and colleagues previously found alternative splicing of *HMGCR*, *HMGCS1*, *MVK*, *PCSK9*,
45   and *LDLR* to be mediated by the splice protein PTBP1 and regulated by cellular cholesterol levels[17].
46   Interestingly, PTBP1 works as an inhibitor of the U2AF splice component, and thus inhibits the
47   recognition of 3' splice sites by the U2-spliceosome[18]. However, the knockdown of *PTBP1* resulted in
48   very limited changes in the expression levels of the different splice forms[17], especially when compared
49   to the drastic changes observed in our study.

50   In our *in vitro* experiments, the knockdown of several U2-spliceosome genes and the resulting
51   IVS3 retention compromised LDLR cell surface expression and LDL uptake as much as the
52   knockdown of *LDLR* itself. The sensitivity of our mass spectrometric analysis only allowed detection

1   of the tagged fragment after overexpression in the immortalized kidney cell line HEK293T. The
2   artificial construct unlike an endogenously produced protein may have escaped nonsense-mediated
3   decay. Nevertheless, we cannot rule out that the theoretical 116 amino acid long aminoterminal
4   fragment of the differentially spliced *LDLR* is expressed *in vivo* and secreted. In fact, human plasma
5   contains LDLR fragments, which are currently assumed to result from shedding of LDLR at the cell
6   surface[19] but may also correspond to secreted alternative splice variants.

7   The relative expression of *LDLR's* IVS3 transcript in human liver varies strongly due to both
8   analytical and biological reasons, namely between 0.4% and 29% upon RNA sequencing, between
9   7.5% and 81% upon chip array analysis, and between 23% and 85% upon qRT-PCR. Very likely,
10   RNA sequencing yielded the most realistic data, because this method recorded the different LDLR
11   transcripts most comprehensively. The large interindividual variation of IVS3 expression recorded by
12   each method indicates relevant regulatory mechanisms and consequences. We made seemingly
13   contradictory findings on the association of IVS3 retention with NAFLD. On the one hand, the
14   percentage of IVS3 transcripts was significantly higher in 30 patients with NAFLD or NASH than in
15   25 normal weight and obese control subjects without NAFLD. On the other hand, the chip array
16   analysis found significant increases of IVS3 transcripts after bariatric surgery, which rather causes
17   regression of NAFLD. However, although causing regression of NASH, bariatric surgery may not
18   necessarily undo all regulatory abnormalities associated with NAFLD. In this regard it is noteworthy,
19   that neither RNA sequencing nor chip array analysis found any significant effect of NASH on IVS3
20   retention (figures 5B and S8d). Larger studies are hence needed to answer the question how NAFLD
21   influences the expression of functional and non-functional *LDLR* transcripts.

22   In peripheral blood cells but not in liver tissue, we found a significant correlation between
23   plasma LDL-C levels and the IVS3 retention *LDLR* transcript, which was stronger than the correlation
24   with the full-length *LDLR* transcript. Smaller sample size and narrower range of LDL-C levels but also
25   differences between tissues may be the reasons, why no significant correlations of LDL-C with any
26   hepatic LDLR transcript expression were found. However, the associations of *RBM25* SNPs with
27   differences in *RBM25* expression and LDL-C levels and the higher than expected prevalence of rare
28   *RBM25* loss of function variants in FH patients with no mutation in canonical FH genes suggest that the
29   regulation of *LDLR* splicing by the U2-spliceosome contributes to the determination of LDL-C levels
30   in humans.

31   The lack of association of hypercholesterolemia with rare variants of any other U2- spliceosome
32   gene may reflect their intolerance to gross variation as suggested by pLI values close to 1. Also of note,
33   the analysis of WES data from the UK biobank only retrieved heterozygous mutations in U2-
34   spliceosome genes whereas our knockdown experiments rather mimic homozygous conditions.
35   Opposite effects on upstream regulators of *LDLR* may be another reason why the majority of SNPs and
36   rare exome variants of the spliceosome genes do not show any association with LDL-C levels. The
37   exclusive association of LDL-C with *RBM25* variants may also indicate that RBM25 regulates LDL-C
38   levels by mechanisms unrelated to the U2-spliceosome and the intron 3 retention. In fact, RBM25 also
39   partakes in other spliceosomal subunits[20]. Of note, RNAi with *RBM25* had the weakest effects on *LDLR*
40   splicing and overexpression of hypercholesterolemia associated *RBM25* mutants in Huh-7 cells resulted
41   in lower LDL uptake without affecting the expression of the *LDLR* IVS3 transcript.

42   The correlation between ENST00000557958 expression in blood cells with age makes us
43   hypothesize that age-related changes in the activity of the U2-spliceosome contributes to the increase
44   in LDL-C that parallels ageing[21] but is not mechanistically understood. The functionality of the
45   splicing process changes with ageing[22]. Somatic mutations or decreased expression of splice factor
46   genes, notably *SF3B1* and *RBM25* have been implicated in age-related processes, including cancer[22,23].
47   The total number of alternatively spliced genes also increases with age[24]. Until recently, *SIRT1* is the
48   only known gene involved in cholesterol metabolism and atherosclerosis[25] whose alternative splicing
49   may be disrupted with age[22]. One may speculate that either the epigenetic dysregulation of the activity
50   of splice factor genes or the accumulation of somatic loss of function variants in liver cells may
51   promote increases in LDL-C with age.

52   Our study has several strengths and limitations. First, our screening unravelled several novel
53   candidate genes that regulate hepatic LDL uptake but missed canonical LDL uptake regulating genes

1   such as *MYLIP*, *MBTPS1*, *PCSK9* or *SREBBP2*. A general reason is the not optimal signal to noise
2   ratio of our screening. A specific reason for missing *MYLIP* or *PCSK9* is the optimization of our
3   screening towards the discovery of loss of function effects. Second, our validation studies did not only
4   confirm the limiting effect of U2-spliceosome genes on LDL uptake but unravelled a novel
5   mechanism of LDL receptor regulation, namely IVS3 retention within an *LDLR* transcript which is
6   translated into a truncated and non-functional receptor protein. In both human liver and peripheral
7   blood cells, we demonstrate that this process happens at considerable quantity and interindividual
8   variability, possibly influenced by aging and NAFLD. Third, *RBM25* was the only spliceosome gene
9   affected by mutations associated with differences in LDL-C, perhaps because *RBM25* may tolerate
10   loss of function better than other U2-spliceosome genes. However, we cannot rule out that RBM25
11   affects LDL metabolism beyond or even independently of *LDLR* splicing because both knockdown of
12   *RBM25* and overexpression of loss of function mutants associated with hypercholesterolemia exerted
13   in Huh-7 cells stronger and more consistent effects on LDL uptake than on IVS3 retention in *LDLR*.

14   In conclusion, we identified IVS3 retention of *LDLR* upon loss of U2-spliceosome activity as
15   a novel mechanism regulating LDLR activity in cells. The importance of this mechanism for the
16   regulation of plasma LDL-C levels and thus determination of cardiovascular risk remains to be
17   established by further studies.

18

Disclosures

1   **Supplemental Materials**
2   Materials & Methods
3   Online Figures S1 to S11
4   Online Tables S1 to S12
5   Major Resource Table
6   Original Western Blots

7
8

1   **Table 1. Hit genes that induced upon knockdown in Huh-7 cells either a decrease (left column)**
2   **or an increase (right column) in LDL uptake.**

	Decreased LDL uptake				Increased LDL uptake		
Gene	**Assay score[A] avg[B]**	**Assay score[A] SEM[C]**	**RSA p-value[D]**	**Gene**	**Assay score[A] avg[B]**	**Assay score[A] SEM[C]**	**RSA p-value[D]**
AP2M1	-3.103179681	0.346648222	$3.36*10^{-8}$	*PROX1*	6.53057396	0.631260417	$3.19*10^{-9}$
CHMP2A	-3.130900347	0.359445533	$2.51*10^{-7}$	*ITGAV*	7.431175355	1.519558432	$2.96*10^{-8}$
NFKB2	-2.59157417	0.136886566	$8.07*10^{-7}$	*TGFBR1*	3.464028514	0.397588943	$7.31*10^{-6}$
***AQR*[E]**	-2.484868551	0.199482589	$4.57*10^{-6}$	*CDC37*	3.747034032	1.072191825	$2.35*10^{-5}$
PSMD11	-2.557101583	0.239773488	$4.77*10^{-6}$	*DTNBP1*	57.92944887	57.2617451	$4.46*10^{-5}$
SF3B2	-2.107311389	0.015210399	$4.81*10^{-6}$	*CYP27C1*	32.06817221	31.61438081	$8.92*10^{-5}$
RPL35	-2.346954606	0.150946677	$5.45*10^{-6}$	*PNPLA2*	2.279278207	0.266420784	$1.26*10^{-4}$
PSMD8	-2.988677308	0.491086915	$6.34*10^{-6}$	*C22orf39*	7.995494448	8.342242785	$1.78*10^{-4}$
SON	-2.164748153	0.201099955	$1.46*10^{-5}$	*TMEM133*	3.049034762	1.060165442	$1.84*10^{-4}$
COPA	-2.307675328	0.213018879	$1.61*10^{-5}$	*TMEM130*	6.466491664	5.317700355	$2.23*10^{-4}$
RBM25	-1.993998657	0.055265194	$1.92*10^{-5}$	*PM20D2*	2.155202336	0.176491898	$2.29*10^{-4}$
RBM22	-2.818121291	0.622885617	$3.36*10^{-5}$	*PET117*	3.001069341	1.652765441	$2.68*10^{-4}$
PSMD3	-2.21302629	0.224903034	$3.98*10^{-5}$	*CWF19L2*	3.806757511	4.571696977	$3.12*10^{-4}$
SF3B5	-2.285064158	0.25878823	$4.32*10^{-5}$	*ENY2*	2.420424347	0.514153659	$3.28*10^{-4}$
SF3B1	-2.267932169	0.253122099	$4.55*10^{-5}$	*NME4*	2.711491413	0.954425612	$3.39*10^{-4}$
SALL4	-1.937993523	1.13065979	$6.02*10^{-5}$	*ZC3H4*	4.545156994	3.551478266	$3.57*10^{-4}$
RPL5	-2.106905493	0.373542859	$7.40*10^{-5}$	*WASF2*	2.310874515	0.449202822	$3.61*10^{-4}$
CCDC180	-1.132459235	1.398333381	$9.52*10^{-5}$	*HELZ2*	2.546828237	0.984740435	$3.87*10^{-4}$
SF3B6	-2.277000896	0.332074616	$9.83*10^{-5}$	*RILP*	1.995550072	0.267567916	$4.23*10^{-4}$
HNRNPU	-1.724036435	0.093847304	$1.23*10^{-4}$	*MAT2A*	3.705559066	3.611891772	$4.91*10^{-4}$
RPL17	-2.226845162	0.329575956	$1.46*10^{-4}$	*NRM*	1.710898743	0.050727817	$5.02*10^{-4}$
ISY1	-2.74487386	0.698388989	$1.55*10^{-4}$	*CEP295NL*	2.189792071	0.474598108	$5.02*10^{-4}$
ZNF641	-1.034460324	1.453444444	$2.58*10^{-4}$	*ACSM2A*	2.207444199	1.531809937	$5.32*10^{-4}$
COPB1	-1.693933632	0.103029465	$2.64*10^{-4}$	*RTL9*	3.759306708	3.473297986	$5.35*10^{-4}$
SF3A1	-2.225755015	0.412106586	$2.72*10^{-4}$	*KIAA1522*	3.362058267	3.27466253	$6.25*10^{-4}$
SNW1	-1.76539067	0.142531611	$2.76*10^{-4}$	*ZNF84*	2.204388764	0.765657329	$6.55*10^{-4}$
EIF2S1	-1.486721463	0.790741651	$3.45*10^{-4}$	*TFAP4*	3.032765033	3.340175625	$6.69*10^{-4}$
CCDC73	-1.041204586	1.27682775	$3.50*10^{-4}$	*TMEM182*	3.227517874	1.666669492	$7.29*10^{-4}$
RPL9	-1.715182797	0.249911985	$3.55*10^{-4}$	*WDR55*	1.967286849	1.365170916	$7.32*10^{-4}$
NXNL2	-1.199311468	1.135835784	$3.83*10^{-4}$	*DYNLL1*	2.268266743	0.467997927	$7.72*10^{-4}$
WBP11	-1.50591484	0.062444555	$4.03*10^{-4}$	*ADPRHL2*	2.078229013	0.322800093	$8.51*10^{-4}$
C2CD5	-1.097951788	1.954971449	$4.46*10^{-4}$	*ELAVL1*	1.945364959	0.968117905	$8.70*10^{-4}$
RPL21	-1.655773242	0.156797718	$4.72*10^{-4}$	*CFAP298*	1.883199038	0.378258022	$8.87*10^{-4}$
EPOP	-1.837314819	0.25795876	$4.80*10^{-4}$	*PMM1*	2.80926863	3.200260012	$8.92*10^{-4}$
RMND5B	-1.523957521	0.076773849	$5.07*10^{-4}$	*CASKIN2*	1.681223061	0.149986926	$9.07*10^{-4}$
TAPBPL	-1.52965773	0.154207886	$5.27*10^{-4}$	*CIZ1*	3.454694336	2.803876145	$9.37*10^{-4}$
STARD10	-1.527795273	0.115135889	$5.45*10^{-4}$	*BRICD5*	1.962503862	0.408074057	$9.41*10^{-4}$
PSMD1	-2.207116523	0.551747426	$5.63*10^{-4}$				
PFDN6	-0.881689024	1.740601376	$5.80*10^{-4}$				

PSMA1	-1.528976301	0.119805079	5.85*10⁻⁴				
RTF2	-1.573924771	0.169765686	6.14*10⁻⁴				
LSM2	-1.448888015	0.056454941	6.40*10⁻⁴				
UBD	-1.171691024	1.530009178	6.69*10⁻⁴				
LRRC14	-1.258311764	1.067910962	6.84*10⁻⁴				
SUPT6H	-1.451332382	0.095214513	7.27*10⁻⁴				
COPB2	-2.037140764	0.468882876	7.34*10⁻⁴				
_SF3A2_	-1.347147433	0.758462926	7.89*10⁻⁴				
ATP6V0C	-1.823918839	0.263639476	7.90*10⁻⁴				
EMILIN3	-1.598631472	2.238859705	8.03*10⁻⁴				
DMTN	-1.559252376	0.142024687	8.20*10⁻⁴				
MRPL19	-0.755460842	1.688052373	8.92*10⁻⁴				
MRO	-0.986783025	1.102624895	9.14*10⁻⁴				
DDX59	-1.380513222	1.040634076	9.25*10⁻⁴				
PSMD12	-1.761325035	0.367766123	9.45*10⁻⁴				

1   [A]Assay score: normalized score for the median cytoplasm intensity assay feature. [B]Avg = average.
2   [C]SEM: standard error of the mean.
3   [D] p-values are not adjusted for multiple testing (p <3.6*10⁻⁶ after Bonferroni adjustment for 14'000
4   genes with expressed transcripts)
5   [E] The 15 hit genes involved in RNA splicing and validated in this study are highlighted in bold and
6   underlined.
7
8
9
10
11

1 **Figure Legends**
2 **Figure 1. Identification and validation of U2-spliceosome genes as limiting factors for the uptake**
3 **of LDL by Huh-7 cells. A. Schematic representation** of the genome-wide image-based siRNA
4 screening and data analysis process. **B. Functional association networks** for genes decreasing LDL
5 uptake upon siRNA-mediated knockdown. Genes with $P < 1.0*10^{-3}$ for median cytoplasm intensity were
6 selected as top hits. Spheres represent single genes. Edges represent known and predicted gene-gene
7 relationships such as protein-protein interactions, co-expression and homology. The graph was produced
8 using the STRING online tool (http://string-db.org/). The superimposed coloured circles are used to
9 highlight the main functional clusters. **C and D. Effects of RNA-interference with U2-spliceosome**
10 **genes on cell association of ^{125}I-LDL in Huh-7 cells.** 72 hours after transfection with siRNAs from
11 Ambion (*LDLR*), Sigma (*RBM25*), or Dharmacon (all other genes)**,** cells were incubated for 2 hours at
12 37°C in the presence of 33.3 μg/mL of ^{125}I-LDL in the presence or absence of 40x excess unlabelled
13 LDL. Specific cell association was calculated as the difference between the two conditions. The data are
14 expressed as means ±SD of 2 quadruplicate experiments. Statistical analysis was performed using
15 Kruskal-Wallis test with Dunn's multiple comparisons test between the non-targeting (scrambled) and
16 each targeting siRNA (**C**) or Mann-Whitney test (one-sided) between each vendor's targeting and non-
17 targeting (scrambled) siRNAs (**D**). The respective p values are shown above each condition.
18
19 **Figure 2. Loss of U2-spliceosome genes causes intron 3 retention in *LDLR*. A**. ***LDLR* Exon level**
20 **expression upon *AQR* knockdown.** Expression of the *LDLR* exons was recorded by RNA sequencing
21 of Huh-7 cells 72 hours after knockdown of *AQR*. Segments represent differential exon usage in each
22 sector of the *LDLR* genomic sequence as identified by the DEXSeq algorithm and as summarized in the
23 linear representation below the graph. Canonical exons of the ENST00000252444 full length transcript
24 are shown below the graph. Normalized read counts are reported on the y axis. The black arrow indicates
25 the location of ENSG00000130164:E009, corresponding to the first half of intron 3. Data represent the
26 average of three independent experiments. **B. ENSG00000130164:E009 is most strongly upregulated**
27 **upon RNA interference with spliceosome genes.** Log2 fold change in gene expression at the exon
28 level for the whole transcriptome after knockdown of *AQR* (x axis), and *SF3B1* (y axis) and *SF3A2* (z
29 axis) in Huh-7 cells. The red circle highlights the position of ENSG00000130164:E009 corresponding
30 to the first half of intron 3. **C. Correlation between LDLR intron 3 retention and LDL cell**
31 **association.** Correlation between the log2 fold change in ENSG00000130164:E009 expression level
32 and the decrease in ^{125}I-LDL cell association (same data as in Figure 1C) upon knockdown of each U2-
33 spliceosome hit gene. Cells treated with a non-targeting siRNA were used as reference. Cell association
34 is expressed as mean±SD. r and p-value were calculated according to Spearman.
35
36 **Figure 3. Determination of LDLR intron 3 splice patterns. A. Cloning strategy and structure of**
37 **the minigenes.** The upper part of this panel shows the genomic location of the two segments of the
38 LDLR gene that were cloned in each minigene, while the lower half shows a simplified structure of the
39 pSPL3 minigene used to express them. Genomic coordinates refer to the hg19 assembly. Note that, due
40 to primer design, MG_1 is 1 bp shorter at its 5' end, starting at chr19:11,212,960. **B. Characterization**
41 **of the splice products.** The graphs represent the mean RNA sequencing coverage at the Exon 3-Intron
42 3 junction in two replicate samples for each condition. Coverage data were normalized to the average
43 coverage for exon 3. MG_1/MG_2 = short / long minigene. **C. *In silico* BPS predictions for the acceptor**
44 **site of *LDLR* exon 4.** BP score: final score (svm_score) according to the SVM-BP-finder algorithm for
45 the putative BPS sequence highlighted in red. A BPS is considered valid when located close to the AG
46 exclusion zone, with BP-score > 0 and with svm_score > 0.
47
48 **Figure 4. Effect of loss of spliceosome function on LDLR protein expression A. Schematic**
49 **structure of the LDLR protein.** (modified from[7]). LDLRret: intron 3 retention fragment, LBD: Ligand
50 binding domain; L1-L7: LDLR class A domain; EGFPH: Epidermal growth factor precursor homology
51 domain; β: beta propeller; O: O-linked sugar repeat; A/B/C: EGF-type repeat; TM: transmembrane
52 domain. The red line represents the location of the last canonical amino acid found also in the LDLRret
53 fragment, followed by 12 novel amino acids and by a stop codon. **B and C. Effect of *SF3B1* and *AQR***
54 **knockdown on LDLR protein levels.** LDLR protein levels in Huh-7 cells 72 hours after *SF3B1* or *AQR*

1 knockdown. **B** shows a representative Western blot. **C,** shows the relative densities of LDLR bands
2 normalized to TATA-binding-protein (TBP, loading control) after knockdown of *AQR* or *SF3B1* relative
3 to the non-targeting control. The data are shown as means ±SD of 3 independent experiments. **D. Effect**
4 **of *SF3B1* and *AQR* knockdown on LDLR cell surface levels.** LDLR cell surface levels in alive Huh-
5 7 cells were measured by flow cytometry 72 hours after knockdown of *SF3B1* or *AQR*. siRNAs against
6 *LDLR* were used as positive controls. The data are normalized to a non-targeting control and are shown
7 as means±SD of 3 independent experiments. Numbers in **C** and **D** are p-values obtained by Kruskal-
8 Wallis test with Dunn's multiple comparisons test between the non-targeting (scrambled) and respective
9 targeting siRNA. **E-F. Overexpressed LDLRret fragment is retrieved in cell lysates and cell culture**
10 **medium.** 48 hours after transfection in HEK293T cells, the HA-tagged version of the LDLRret fragment
11 was detected-by western blot in both total cell lysates **(E, F)** and media **(F)**. Lysates after 2 and more
12 hours of incubation were obtained after treatment with the proteasome inhibitor MG132 as indicated by
13 the labels in **(E)**. EV = pcDNA3.1 empty vector. HA-frag = hemagglutinin-tagged LDLRret fragment.
14
15 **Figure 5. *LDLR* intron 3 retention in human liver. A. Detection of intron 3 retention in human**
16 **liver by qRT-PCR.** Transcripts encoding full-length *LDLR* or the IVS3 retention variant were
17 measured by qRT-PCR and normalized to GAPDH mRNA levels in healthy liver tissue of 17 patients
18 with benign liver tumours and in liver biopsies of 9 patients with suspected NAFLD. Each bar shows
19 the relative expression of the two *LDLR* transcripts in one subject. **B and C**. **Percent expression of**
20 **the *LDLR* transcript *LDLR-206* with retention of intron 3 (B) and a full length *LDLR* transcript**
21 ***LDLR-208* (C) relative to the sum of all 14 *LDLR* transcripts in livers of 13 healthy subjects or 12**
22 **obese patients without non-alcoholic fatty liver disease (NAFLD), 15 patients with NAFLD and**
23 **15 patients with non-alcoholic steatohepatitis (NASH).** Computational analysis of previously
24 published RNA sequencing data (Gene Expression Omnibus, accession number GSE126848)[8]. For all
25 transcripts, see figure S7. The dark and light blue lines within the violin plots represent means and
26 medians, respectively. Numbers indicate p values obtained by comparisons of indicated groups using
27 the Kruskal-Wallis test and adjusted for multiple testing using the Bonferroni correction. **D.**
28 **Expression of *LDLR* exons and introns in human liver.** The violin plots show the normalized signal
29 intensities for probes mapping to the 5'-UTR, 3'-UTR, the exons and some introns of the LDLR gene
30 in 155 obese non-diabetic subjects. Dots indicate median values. Error bars span from the 2.5th to the
31 97.5th percentile. Intron 3 is highlighted in red while the other introns are shown in grey. The location
32 of each probe is depicted in the diagram below.
33
34 **Figure 6. Correlations of the *LDLR* ENST00000557958 (A, B) and ENST00000252444 transcripts**
35 **(C, D) in whole blood samples with age (A, C) and LDL-C levels (B, D).** Data is from 2,462 subjects
36 of the BIOS population[10]. ENST00000557958 represents the intron 3 retention transcript **(A, B)**.
37 ENST00000252444 **(C, D)** was the only full length *LDLR* transcript detected in all samples analysed. r
38 values and p values (adjusted for multiple testing using the Bonferroni correction) refer to a Spearman
39 correlation analysis. Linear regression lines and their 95% confidence intervals are shown in blue and
40 gray, respectively.
41
42 **Figure 7. Association between *RBM25* variants and LDL-C in the UK Biobank dataset. A.**
43 **Association of GWAS SNPs from 11 spliceosome genes with LDL-C in the UK Biobank dataset.**
44 The dashed red horizontal line indicates the threshold for statistical significance after Bonferroni
45 correction for multiple testing of 1,360 variants within the genes of interest ($p=3.7*10^{-5}$). Effect size and
46 directionality are reported on the x axis as beta value. **B. Association between the rs17570658**
47 **genotype and *RBM25* expression in different tissues.** Data shown for skeletal muscle and tibial artery
48 (both empirical $p < 1.0*10^{-8}$ corrected for multiple testing across genes using Storey's q value
49 method[26,27]). The horizontal white lines reflect medians; the upper and lower borders of the grey boxes
50 reflect the 75th and 25th percentiles, respectively.
51
52

References

1. Ference BA, Ginsberg HN, Graham I, Ray KK, Packard CJ, Bruckert E, Hegele RA, Krauss RM, Raal FJ, Schunkert H, et al. Low-density lipoproteins cause atherosclerotic cardiovascular disease. 1. Evidence from genetic, epidemiologic, and clinical studies. A consensus statement fromthe European Atherosclerosis Society Consensus Panel. Eur. Heart J. 2017;38:2459–2472.

2. Zanoni P, Velagapudi S, Yalcinkaya M, Rohrer L, von Eckardstein A. Endocytosis of lipoproteins. Atherosclerosis. 2018;275:273–295.

3. Wilkinson ME, Charenton C, Nagai K. RNA Splicing by the Spliceosome [Internet]. Annu. Rev. Biochem. 2020;89:359–388.

4. Emmer BT, Sherman EJ, Lascuna PJ, Graham SE, Willer CJ, Ginsburg D. Genome-scale CRISPR screening for modifiers of cellular LDL uptake. PLoS Genet. 2021;17:e1009285.

5. Cameron J, Holla ØL, Kulseth MA, Leren TP, Berge KE. Splice-site mutation c.313+1, G>A in intron 3 of the LDL receptor gene results in transcripts with skipping of exon 3 and inclusion of intron 3. Clin. Chim. Acta. 2009;403:131–135.

6. Corvelo A, Hallegger M, Smith CWJ, Eyras E. Genome-wide association between branch point properties and alternative splicing. PLoS Comput. Biol. 2010;6:e1001016.

7. Surdo P Lo, Bottomley MJ, Calzetta A, Settembre EC, Cirillo A, Pandit S, Ni YG, Hubbard B, Sitlani A, Carfí A. Mechanistic implications for LDL receptor degradation from the PCSK9/LDLR structure at neutral pH. EMBO Rep. 2011;12:1300–1305.

8. Suppli MP, Rigbolt KTG, Veidal SS, Heebøll S, Eriksen PL, Demant M, Bagger JI, Nielsen JC, Oró D, Thrane SW, et al. Hepatic transcriptome signatures in patients with varying degrees of nonalcoholic fatty liver disease compared with healthy normal-weight individuals. Am. J. Physiol. - Gastrointest. Liver Physiol. 2019;316:G462–G472.

9. Lefebvre P, Lalloyer F, Baugé E, Pawlak M, Gheeraert C, Dehondt H, Vanhoutte J, Woitrain E, Hennuyer N, Mazuy C, et al. Interspecies NASH disease activity whole-genome profiling identifies a fibrogenic role of PPARα-regulated dermatopontin. J. Clin. Invest. 2017;2:1–17.

10. Zhernakova D V., Le TH, Kurilshikov A, Atanasovska B, Bonder MJ, Sanna S, Claringbould A, Võsa U, Deelen P, Franke L, et al. Individual variations in cardiovascular-disease-related protein levels are driven by genetics and gut microbiome. Nat. Genet. 2018;50:1524–1532.

11. Cirulli ET, White S, Read RW, Elhanan G, Metcalf WJ, Tanudjaja F, Fath DM, Sandoval E, Isaksson M, Schlauch KA, et al. Genome-wide rare variant analysis for thousands of phenotypes in over 70,000 exomes from two cohorts. Nat. Commun. 2020;11:542.

12. Lek M, Karczewski KJ, Minikel E V., Samocha KE, Banks E, Fennell T, O'Donnell-Luria AH, Ware JS, Hill AJ, Cummings BB, et al. Analysis of protein-coding genetic variation in 60,706 humans. Nature. 2016;536:285–291.

13. Liu DJ, Peloso GM, Yu H, Butterworth AS, Wang X, Mahajan A, Saleheen D, Emdin C, Alam D, Alves AC, et al. Exome-wide association study of plasma lipids in >300,000 individuals. Nat. Genet. 2017;49:1758–1766.

14. Willer CJ, Li Y, Abecasis GR. METAL: Fast and efficient meta-analysis of genomewide association scans. Bioinformatics. 2010;26:2190–2191.

15. Futema M, Plagnol V, Li K, Whittall RA, Neil HAW, Seed M, Bertolini S, Calandra S, Descamps OS, Graham CA, et al. Whole exome sequencing of familial hypercholesterolaemia patients negative for LDLR / APOB / PCSK9 mutations. J. Med. Genet. 2014;51:537–544.

16. Kraehling JR, Chidlow JH, Rajagopal C, Sugiyama MG, Fowler JW, Lee MY, Zhang X, Ramírez CM, Park EJ, Tao B, et al. Genome-wide RNAi screen reveals ALK1 mediates LDL uptake and transcytosis in endothelial cells. Nat. Commun. 2016;7:13516.

17. Medina MW, Krauss RM. Alternative splicing in the regulation of cholesterol homeostasis. Curr. Opin. Lipidol. 2013;24:147–52.

18. Shao C, Yang B, Wu T, Huang J, Tang P, Zhou Y, Zhou J, Qiu J, Jiang L, Li H, et al. Mechanisms for U2AF to define 3′ splice sites and regulate alternative splicing in the human genome. Nat. Struct. Mol. Biol. 2014;21:997–1005.

19. Mayne J, Ooi TC, Tepliakova L, Seebun D, Walker K, Mohottalage D, Ning Z, Abujrad H, Mbikay M, Wassef H, et al. Associations between Soluble LDLR and Lipoproteins in a White Cohort and the Effect of PCSK9 Loss-of-Function. J. Clin. Endocrinol. Metab. 2018;103:3486–3495.

1   20. Carlson SM, Soulette CM, Yang Z, Elias JE, Brooks AN, Gozani O. RBM25 is a global
2   splicing factor promoting inclusion of alternatively spliced exons and is itself regulated by
3   lysine mono-methylation. J. Biol. Chem. 2017;292:13381–13390.
4   21. Balder JW, de Vries JK, Nolte IM, Lansberg PJ, Kuivenhoven JA, Kamphuisen PW. Lipid and
5   lipoprotein reference values from 133,450 Dutch Lifelines participants: Age- and gender-
6   specific baseline lipid values and percentiles. J. Clin. Lipidol. 2017;11:1055-1064.e6.
7   22. Deschênes M, Chabot B. The emerging role of alternative splicing in senescence and aging
8   [Internet]. Aging Cell. 2017;16:918–933.
9   23. Seiler M, Peng S, Agrawal AA, Palacino J, Teng T, Zhu P, Smith PG, Buonamici S, Yu L,
10   Caesar-Johnson SJ, et al. Somatic Mutational Landscape of Splicing Factor Genes and Their
11   Functional Consequences across 33 Cancer Types. Cell Rep. 2018;23:282-296.e4.
12 24. Rodríguez SA, Grochová D, Mckenna T, Borate B, Trivedi NS, Erdos MR, Eriksson M. Global
13   genome splicing analysis reveals an increased number of alternatively spliced genes with
14   aging. Aging Cell. 2016;15:267–278.
15 25. Miranda MX, Van Tits LJ, Lohmann C, Arsiwala T, Winnik S, Tailleux A, Stein S, Gomes AP,
16   Suri V, Ellis JL, et al. The Sirt1 activator SRT3025 provides atheroprotection in Apoe-/- mice
17   by reducing hepatic Pcsk9 secretion and enhancing Ldlr expression. Eur. Heart J. 2015;36:51–
18   59.
19 26. Aguet F, Brown AA, Castel SE, Davis JR, He Y, Jo B, Mohammadi P, Park YS, Parsana P,
20   Segrè A V., et al. Genetic effects on gene expression across human tissues. Nature.
21   2017;550:204–213.
22 27. Storey JD, Tibshirani R. Statistical significance for genomewide studies. Proc. Natl. Acad. Sci.
23   U. S. A. 2003;100:9440–9445.
24 28. Havel RJ, Eder HA, Bragdon JH. The distribution and chemical composition of
25   ultracentrifugally separated lipoproteins in human serum. J. Clin. Invest. 1955;34:1345–1353.
26 29. Velagapudi S, Yalcinkaya M, Piemontese A, Meier R, Nørrelykke SF, Perisa D, Rzepiela A,
27   Stebler M, Stoma S, Zanoni P, et al. VEGF-A regulates cellular localization of SR-BI as well
28   as transendothelial transport of HDL but Not LDL. Arterioscler. Thromb. Vasc. Biol.
29   2017;37:794–803.
30 30. McFarlane AS. Efficient trace-labelling of proteins with iodine. Nature. 1958;182:53.
31 31. Kamentsky L, Jones TR, Fraser A, Bray MA, Logan DJ, Madden KL, Ljosa V, Rueden C,
32   Eliceiri KW, Carpenter AE. Improved structure, function and compatibility for cellprofiler:
33   Modular high-throughput image analysis software. Bioinformatics. 2011;27:1179–1180.
34 32. Parsons BD, Schindler A, Evans DH, Foley E. A Direct Phenotypic Comparison of siRNA
35   Pools and Multiple Individual Duplexes in a Functional Assay. PLoS One. 2009;4:e8471.
36 33. Bolger AM, Lohse M, Usadel B. Trimmomatic: A flexible trimmer for Illumina sequence data.
37   Bioinformatics. 2014;30:2114–2120.
38 34. Dobin A, Davis CA, Schlesinger F, Drenkow J, Zaleski C, Jha S, Batut P, Chaisson M,
39   Gingeras TR. STAR: Ultrafast universal RNA-seq aligner. Bioinformatics. 2013;29:15–21.
40 35. Liao Y, Smyth GK, Shi W. The Subread aligner: Fast, accurate and scalable read mapping by
41   seed-and-vote. Nucleic Acids Res. 2013;41:e108.
42 36. Anders S, Reyes A, Huber W. Detecting differential usage of exons from RNA-seq data.
43   Genome Res. 2012;22:2008–2017.
44 37. Fedoseienko A, Wijers M, Wolters JC, Dekker D, Smit M, Huijkman N, Kloosterhuis N, Klug
45   H, Schepers A, van Dijk KW, et al. The COMMD family regulates plasma LDL levels and
46   attenuates atherosclerosis through stabilizing the CCC complex in endosomal LDLR traffcking.
47   Circ. Res. 2018;122:1648–1660.
48 38. MacLean B, Tomazela DM, Shulman N, Chambers M, Finney GL, Frewen B, Kern R, Tabb
49   DL, Liebler DC, MacCoss MJ. Skyline: An open source document editor for creating and
50   analyzing targeted proteomics experiments. Bioinformatics. 2010;26:966–968.
51 39. Nisson PE, Watkins PC, Krizman DB. Isolation of exons from cloned DNA by exon trapping.
52   Curr. Protoc. Hum. Genet. 2001;Chapter 6:Unit 6.1.
53 40. Bray NL, Pimentel H, Melsted P, Pachter L. Near-optimal probabilistic RNA-seq
54   quantification. Nat. Biotechnol. 2016;34:525–527.
55 41. Cirulli, E.T. and Washington NL. Helix Research. UK Biobank Exome rare variant analysis

1   v1.3 [Internet]. Helix Blog.

2 42. Whiffin N, Minikel E, Walsh R, O'Donnell-Luria AH, Karczewski K, Ing AY, Barton PJR,
3   Funke B, Cook SA, Macarthur D, et al. Using high-resolution variant frequencies to empower
4   clinical genome interpretation. Genet. Med. 2017;19:1151–1158.

5 43. Birmingham A, Selfors LM, Forster T, Wrobel D, Kennedy CJ, Shanks E, Santoyo-Lopez J,
6   Dunican DJ, Long A, Kelleher D, et al. Statistical methods for analysis of high-throughput
7   RNA interference screens. Nat. Methods. 2009;6:569–75.

8 44. König R, Chiang C, Tu BP, Yan SF, DeJesus PD, Romero A, Bergauer T, Orth A, Krueger U,
9   Zhou Y, et al. A probability-based approach for the analysis of large-scale RNAi screens. Nat.
10   Methods. 2007;4:847–849.

11 45. Roweis ST, Saul LK. Nonlinear dimensionality reduction by locally linear embedding. Science
12   (80-.). 2000;290:2323–2326.

13

14

Novelty and Significance

What Is Known?

- The low density lipoprotein (LDL) receptor (LDLR) regulates LDL-cholesterol levels in blood by mediating the uptake of LDL into hepatocytes
- The transcriptional and posttranslational regulation of LDLR activity is targeted by cholesterol lowering drugs

What New Information Does This Article Contribute?

- Loss of subunits or interactors of the U2 spliceosome decreases the uptake of LDL into Huh7 hepatocarcinoma cells
- Loss of subunits or interactors of the U2 spliceosome cause intron 3 retention of the *LDLR* mRNA and, thereby, loss of LDR function
- Intron 3 retention of *LDLR* in human liver and peripheral blood cells is increased by non-alcoholic fatty liver disease and aging, respectively.
- Single nucleotide polymorphisms of the spliceosome gene *RBM25* are associated with higher *RBM25* expression in tissues and lower LDL-cholesterol
- Expression of rare structural variants of *RBM25* associated with familial hypercholesterolemia decrease LDL-uptake into Huh7 cells

Low density lipoprotein (LDL) cholesterol is a causal and treatable risk factor of atherosclerotic cardiovascular diseases whose plasma level is most strongly determined by hepatic removal through the LDL receptor (LDLR). LDLR activity is known to be regulated both by transcription of the *LDLR* gene and degradation of the LDLR protein. By genome wide RNA interference we identified 15 genes encoding subunits and interactors of the U2 spliceosome to limit the uptake of LDL into Huh7 hepatocarcinoma cells. We identified intron 3 retention of the *LDLR* mRNA as the underlying mechanism. The mRNA expression analysis of human liver samples and peripheral blood cells showed the high interindividual variation of this newly identified post-transcriptional regulation of LDLR. Intron 3 retention increases in non-alcoholic fatty liver disease as well as with ageing. Moreover, genetic variation in the U2 spliceosome gene RBM25 is associated with differences in LDL-cholesterol. Overall, we identified a novel mechanism of LDLR regulation which might help to better understand the etiology and pathophysiology of LDL-hypercholesterolemia.

Figure 1

A.

6 batches, 32 plates/batch

8. *In vitro / In vivo* validation

1. siRNA reverse transfection (t = 0)

2. Lipoprotein internalization assay (t = 72h)

3. Fluorescence microscopy imaging

DAPI   RFP

4. Foci identification and quantification

5. Quality control

6. RSA analysis and hit identification

Positive regulators

Negative regulators

7. Hit clustering and GO analysis

B.

○ Ribosome
○ Proteasome
○ Spliceosome
○ Vesicular transport

C.

^{125}I-LDL Cell association % of Scrambled

LDLR — $5.0 * 10^{-6}$
SF3A1 — $3.6 * 10^{-1}$
SF3A2 — $1.0 * 10^{-6}$
SF3B1 — $2.0 * 10^{-6}$
SF3B2 — $1.5 * 10^{-3}$
SF3B4 — 1.0
SF3B5 — $2.0 * 10^{-1}$
SF3B6 — $3.1 * 10^{-1}$
RBM22 — $4.4 * 10^{-1}$
ISY1 — $2.7 * 10^{-1}$
AQR — $2.0 * 10^{-6}$

D.

^{125}I-LDL cell association % of each scrambled

scrambled (SIGMA)
RBM25 (SIGMA) — $1.6 * 10^{-4}$
scrambled (DHA)
RBM25 (DHA) — $9.7 * 10^{-1}$
scrambled (AMBION)
LDLR(AMBION) — $7.8 * 10^{-5}$

Figure 2

A.

AQR   Scrambled

Expression

E001 E005 E009 E013 E017 E021 E025 E029 E033 E037 E041 E045

DexSeq exon usage

11089362   11099241   11109119   11118998   11128877

ENST00000252444

1   2 3 4 5 6 7 8 9 10 11 12 13 14 15   16 17 18

B.

log2FC SF3B1

log2FC AQR

log2FC SF3A2

C.

^{125}I-LDL Cell association % of Scrambled

SF3B4

ISY1

SF3A1

SF3B2

RBM22

SF3B6   SF3B5

RBM25

SF3A2   AQR   SF3B1

$y = -7.7x + 95.2$
$r = -0.73$
$p = 1.4 * 10^{-2}$

100

80

60

40
40

0

0   2   4   6

ENSG00000130164:E009 log2 fold change

Figure 3

A.

B.

C.

BP score: 0.68379

Homo sapiens 5'-tcacacggtgatggtggtctcggcccatccatccctgc**ag**- Exon 4

BP score: 1.35885

Mus musculus 5'-tagcctgacagggccctctcctccctgtgcacccctgc**ag**- Exon 4

Figure 4

A.

LBD   EGFPH

N   L1   L2 | L3   L4   L5   L6   L7   A   B   β   C   O   TM   C

LDLRret

B.

	Scrambled (DHA)	siAQR (DHA)	siSF3B1 (DHA)	
LDLR				—130kDa
TBP				—35kDa

C.

LDLR protein level, % of scrambled

100

$6.8 * 10^{-2}$

50

$9.7 * 10^{-2}$

0

AQR (DHA)   SF3B1 (DHA)

D.

LDLR cell surface abundance, % of each scrambled

100

50

$6.1 * 10^{-1}$ $4.9 * 10^{-2}$ $2.2 * 10^{-2}$

0

siAQR (DHA)   siSF3B1 (DHA)   siLDLR (AMBION)

E.

	EV	HA-LDLRret fragment				
MG-132 (h)	0	0	2	4	6	8
HA						—15kDa
Beta Actin						—50kDa

F.

		EV	HA-frag	
Total Cell Lysates	HA			—15kDa
	Beta Actin			—50kDa
Media	HA			—20kDa

Figure 5

Figure 6

A.

$$y = 0.011x + 1.2$$
$$r = 0.25, p = 9.2 * 10^{-36}$$

ENST00000557958
(Normalized transcript levels)

Age (years)

B.

$$y = 0.057x + 1.6$$
$$r = 0.089, p = 3.9 * 10^{-5}$$

ENST00000557958
(Normalized transcript levels)

LDL-C (mmol/L)

C.

$$y = 0.0094x + 2.4$$
$$r = 0.19, p = 8.8 * 10^{-20}$$

ENST00000252444
(Normalized Transcript Levels)

Age (years)

D.

$$y = - 0.06x + 3.1$$
$$r = -0.033, p = 4.0 * 10^{-1}$$

ENST00000252444
(Normalized Transcript Levels)

LDL-C (mmol/L)

Figure 7

A.

B.

SUPPLEMENTAL MATERIAL to

Posttranscriptional regulation of the human LDL receptor

by the U2-spliceosome

Paolo Zanoni[1,2,*], Grigorios Panteloglou[1,2,*], Alaa Othman[3], Joel T. Haas[4], Roger Meier[5],

Antoine Rimbert[6], Marta Futema[7], Yara Abou Khalil[8,9], Simon F. Norrelykke[5],

Andrzej J. Rzepiela[5], Szymon Stoma[5], Michael Stebler[5], Freerk van Dijk[10], Melinde Wijers[6],

Justina C. Wolters[6], Nawar Dalila[11], Nicolette C. A. Huijkman[6], Marieke Smit[6],

Antonio Gallo[12], Valérie Carreau[12], Anne Philippi[13], Jean-Pierre Rabès[8,14,15],

Catherine Boileau[8,16], Michele Visentin[17], Luisa Vonghia[18,19], Jonas Weyler[18,19],

Sven Francque[18,19], An Verrijken[19,20], Ann Verhaegen[19,20], Luc Van Gaal[19,20],

Adriaan van der Graaf[10], Belle V. van Rosmalen[21], Jerome Robert[1], Srividya Velagapudi[1,2],

Mustafa Yalcinkaya[1,2], Michaela Keel[1,2], Silvija Radosavljevic[1,2], Andreas Geier[22],

Anne Tybjaerg-Hansen[11], Mathilde Varret[8], Lucia Rohrer[1,2], Steve E. Humphries[23],

Bart Staels[4], Bart van de Sluis[6], Jan Albert Kuivenhoven[6], and Arnold von Eckardstein[#,1,2]

* These authors contributed equally to this work

1. Supplemental Material and Methods

Material

siRNAs, antibodies, cells, as well as sources of data are described in the Major Resource

Table. Sources of all other materials are described in the running text.

Cell culture

Huh7, HepG2 and HEK293T cells were cultured in DMEM (cat. D6546, Sigma-Aldrich,

Buchs, Switzerland) complemented with 10% fetal bovine serum (cat. 10500056, Thermo

Fisher Scientific, Reinach, Switzerland) and penicillin/streptomycin (100 U/mL each, cat.

15140122, Thermo Fisher Scientific).

Quantitative Reverse Transcription Real-Time PCR (qRT-PCR)

Total RNA was extracted using Tri reagent$^{®}$ (cat. T9424, Sigma-Aldrich) and treated with

DNAse I (cat. 04 716 728 001, Roche, Switzerland) according to manufacturer`s instructions.

cDNAs were generated using the RevertAid First Strand Synthesis kit (cat. K1621, Thermo

Fisher Scientific). Quantitative real time PCR reactions were performed on a Roche Light

Cycler 480-II (cat. 05015243001, Roche, Switzerland) using the LightCycler® 480 SYBR

Green I Master (cat. 04887352001, Roche, Switzerland). For each run, the following

thermocycle conditions were used: pre-incubation at 95°C for 5 minutes and 45 cycles of

denaturation at 95°C for 10 seconds, primer annealing at 60°C for 10 seconds and extension

at 72°C for 20 seconds. For each experiment, 3 technical replicates were used for each

condition. At the end of each PCR run, the specificity of the PCR products was confirmed by

melting temperature (T_m) analysis. The data were analyzed by performing relative

quantification based on crossing point (Cp) values for the reference gene (*GAPDH*) and the

gene of interest using the relative standard curve method. For each condition, the ratio of the

signal for each gene of interest / signal *GAPDH* was calculated and the data were normalized

to the respective control condition, as described for each experiment.

Isolation and labeling of plasma lipoproteins

LDL (1.019<d<1.063 kg/L) and HDL (1.063<d<1.21 kg/L) were isolated from frozen human

normolipidemic plasma of blood donors by sequential ultracentrifugation[28] using the

OptimaTM L-90K Ultracentrifuge and the Type 70 Ti fixed angle rotor both from Beckman

Coulter (Brea, USA) and centrifuging at approximately 257,000 g, 15°C for ~16 hours .

Density was adjusted by using a KRUESS DS7000 densitometer (Hamburg, Germany). To

avoid the oxidation of lipoproteins, EDTA was added to a final concentration of 30 mM.

For the genome-wide siRNA screening, LDL and HDL were labeled with Atto594 and

Atto655, respectively (cat. AD594-35 and AD655-35, respectively, Atto-Tec, Siegen,

Germany) -as published before[29]. For validation experiments, we labeled both LDL and HDL

with ^{125}I according to the McFarlane method[29,30].

siRNA genome-wide screening

The genome-wide siRNA screening of genes limiting the uptake of fluorescently labeled LDL

was performed in the Scientific Center for Optical and Electron Microscopy (ScopeM) of

ETH Zurich: https://scopem.ethz.ch/. The Ambion Silencer Select Human Genome siRNA

library V4 (cat. 4397926, Thermo Fisher Scientific) containing three unique, non-overlapping

siRNAs for each of the 21,584 human genes, was diluted in sterile nuclease-free water and re-

plated in 192 BD-Falcon clear bottom 384 wells assay plates (cat. 08-772-151, Thermo Fisher

Scientific). 5µL of an 80 nM solution of each siRNA was plated in each well of the assay

plates maintaining the same layout as in the master library. As internal controls, each of the

following Ambion Silencer Select siRNA oligonucleotides (Thermo Fisher Scientific) were

plated in four replicate wells in each of the 192 assay plates: anti-*PLK1*, anti-*LDLR*, and the

Silencer™ Select Negative Control No. 1 siRNA. The assay plates were sealed and maintained at -20 °C until use. One copy of the entire library was used to perform our screening. Libraries were plated using a Tecan Freedom Evo automated liquid handling robot (Tecan, Männedorf, Switzerland). Liquid handling for the screening was performed by an EL406 liquid handling robot (Bio-Tek Instruments, Luzern, Switzerland).

On Day 1, the assay plates were thawed and spun at 1000g for 3 minutes at room temperature. RNAiMax (cat. 13778150, Thermo Fisher Scientific) was diluted in DMEM (0.075 µL of RNAiMax for each 10 µL of DMEM) and 10 µL of diluted RNAiMax were added to each well. The plates were incubated under these conditions for 1 hour at room temperature. In the meantime, Huh-7 cells were detached by trypsin treatment for 15 minutes at 37°C. After trypsinization, the cells were re-suspended in DMEM 12.3% FBS and counted using a Neubauer chamber. The cells were then diluted to a final concentration of 26,154 cells/mL (corresponding to a final concentration of 1,700 cells/well) in DMEM 12.3% FBS in 5l Double Sidearm CellStar® Spinner Flasks (Wheaton, Millville, NJ, USA) in a water bath set at 37°C. After 5-10 minutes of gentle stirring, 65µl of cell suspension was added to each well and the plates were immediately placed on pre-heated metal blocks in a cell culture incubator set at 37°C, 5% CO_2. The cells were maintained under these conditions for 72 hours. Final siRNA concentration was 5 nmol/L. We will refer to the abovementioned transfection protocol as "reverse transfection" in this manuscript, to indicate that the cell suspension was added at the end of the transfection process.

On Day 4, 60 µL of medium were aspirated from each well, followed by the addition of 20 µL of a solution with 66 µg each of Atto594-LDL and Atto655-HDL protein/mL in DMEM, for a final concentration of 33 µg/mL. After incubation for 4 hours at 37°C, 5% CO_2, the cells of each well were washed six times with PBS, followed by the addition of 50 µL of an isotonic 2% paraformaldehyde solution containing 20 µg/mL of Hoechst 33258 (cat. 861405,

Sigma- Aldrich). After another 15 minutes at room temperature, the cells were washed again six times with PBS to remove the paraformaldehyde. After the last wash, PBS was aspirated and substituted with a 0.05% solution of sodium azide in water. The plates were then sealed with adhesive aluminum foil and kept at 4°C protected from light until imaging.

Imaging was performed by two twin ImageXpress micro HCS microscopes (Molecular Devices, Sunnyvale, CA, USA) fed by a robotic arm and equipped with Photometrics CoolSNAP HQ^2 CCD cameras (Photometrics, Tucson, AZ, USA) and a Lumencor Spectra X solid-state light engine (Lumencor, Beaverton, OR, USA). For each assay plate, two datasets were collected. First, the whole surface of each well was captured at 4x magnification in the DAPI channel for cell counting. Second, 9 tiled sites in each well were then acquired with a 20x objective in the DAPI, RFP and CY5 channels to allow for the final image analysis.

After acquisition, image segmentation and the subsequent image analysis were performed using Cell Profiler (http://cellprofiler.org/, The Broad Institute, Cambridge, MA, USA)[31]. The data were initially recorded for more than 100 different assay features. Based on their close relationship with the phenotype of interest, the number of assay features taken into consideration for further analysis was restricted subsequently to the following five: foci count per cell, foci mean intensity, cytoplasm granularity 1 and 2, cytoplasm median intensity. Furthermore, the "nuclei count" feature was used to measure toxicity as well as to determine transfection efficiency by measuring the extent of cell death induced by knockdown of *PLK1*. Downstream data analysis and hit gene identification was performed using the R statistical software (R-project.org) and applying the procedures described in the statistics section. Hits coming from the 'median cytoplasm intensity' assay feature were selected for validation as this feature displayed the highest Z'-factor values when compared to other assay features. A previous RNA sequencing experiment conducted in similar conditions (see below) was used to exclude hit genes that are not expressed in Huh-7 cells or for whom no expression data could be generated, for example pseudogenes or uncharacterized loci. This led to the

exclusion of 4 ribosomal pseudogenes (namely RPL13AP20, RPL34P34, RPL18AP16 and

RPL21P20) from the hits that led to a decrease in LDL uptake upon knockdown. We also

excluded 6 uncharacterized loci, 1 pseudogene and 10 non expressed genes from the list of

genes that increased uptake upon knockdown.

Validation of the screening hits

The validation experiments in Huh-7 and HepG2 cells were performed in 24-well-plates,

using 4 technical replicates for total cellular association (for explanation please see below)

and 2 technical replicates for the unspecific cellular association, per each condition

respectively, in each experiment. Four pooled siRNA oligonucleotides (Major Resource

Table), against each of the top hits were reverse transfected (see screening methods above)

using Lipofectamine RNAiMax (cat. 13778150, Thermo Fisher Scientific) according to the

manufacturer's instructions. This pooling strategy has been shown to target multiple

transcripts as well as multiple positions within the same transcript at the same time, thus

maximizing knockdown efficiency[32]. The final siRNA concentration after the addition of the

cell suspension was 10 nM. As positive control, *LDLR* was knocked down with siRNA

oligonucleotide from Ambion Silencer Select. For the validation of *RBM25*, siRNAs from

Dharmacon and Sigma were used, because of potential off-target effects of the Dharmacon

anti-RBM25 siRNA (see Results section). Knockdown efficiency was determined by qPCR

using *GAPDH* expression levels as the reference (primers sequences in Table S11). Cell

association of ^{125}I-LDL or ^{125}I-HDL (33.3 μg/mL, 2 hours incubation at 37°C) was recorded

72 hours after transfection as described previously[29]. The cells were incubated with the

respective iodinated lipoprotein without (total) or with 40 times excess of the respective non-

labeled lipoprotein (unspecific). The cells were then washed and lysed using 0.1 M NaOH for

1 hour and the ^{125}I-signal was measured using a Wizard[2]10-Detector Gamma counter (cat.

2470-0100, Perkin Elmer). The protein content of each sample was determined using the

micro-BCA Protein Assay Kit (cat. 23235, Thermo Fisher Scientific) and the ratio of the counts / protein content for each technical replicate of each sample was determined. Specific cellular association was calculated by subtracting the unspecific (mean value of the 2 technical replicates of each condition)) from the total (individual values of each technical replicate-total- of each condition).

RNA Sequencing in Huh-7 cells

In order to identify genes differentially spliced upon knock-down of U2-spliceosome components, Huh-7 cells were first transfected with Dharmacon siRNA pools (see Major Resource Table) in 3 separate replicate experiments according to the same protocol used for cell association studies. 72 hours after transfection, the cells were washed once with PBS. Total RNA was extracted with the Genelute Mammalian Total RNA Miniprep Kit (cat. RTN350, Sigma-Aldrich, Switzerland). Genomic DNA was eliminated by on-column DNase digestion (cat. D2816, Sigma-Aldrich, Switzerland). RNA was then sequenced at the Functional Genomics Center Zurich (https://fgcz.ch/) after poly(A) selection with the TruSeq RNA Library Prep Kit (Illumina, San Diego, CA, USA) on an Illumina HiSeq4000 automated sequencer (Illumina, San Diego, CA, USA) to generate single-end reads of length 126nt. The average read depth was $3.13*10^7$ reads/sample. The raw reads were first cleaned by removing adapter sequences, trimming low quality ends, and filtering reads with low quality (phred quality <20) using Trimmomatic[33]. Sequence alignment of the resulting high-quality reads to the Homo Sapiens reference genome (build GRCh38) was carried out using STAR (Version 2.5.1b)[34]. Basal gene expression was determined by performing the same experiment on non-transfected Huh-7 cells. Gene expression values were computed with the function featureCounts from the Bioconductor package Rsubread[35]. To detect candidates for differential exon usage we used DEXSeq[36]. Sequences can be accessed by codes

PRJEB46899 and PRJEB46898, respectively, in the data bank of the European Nucleotide

Archive (https://www.ebi.ac.uk/ena/browser/support)

Measurement of intron 3 retention by qRT-PCR

Alternative splicing of the segment between exons 3 and 4 of *LDLR* upon knockdown

of spliceosome gene hits in Huh-7 cells as well as in human liver samples (see below) was

studied by qRT-PCR using previously published[5] primer couples annealing in exon 3, intron 3

and exon 4 (see Table S11 for primer sequences).

Molecular cloning and LDLR-ret fragment overexpression

The coding sequence of the LDLR fragment formed after intron 3 retention (LDLRret) was

obtained by PCR amplification of cDNA after *SF3B1* knockdown using the primers listed in

Table S11 and subcloned in pCR-Blunt (Thermo Fisher Scientific, The Netherlands)

according to the manufacturer's instructions. A synthetic oligonucleotide encoding a version

of LDLRret carboxyterminally tagged with hemagglutinin (HA) was obtained through

Invitrogen GeneArtTM StringsTM DNA Fragments (Thermo Fisher Scientific) and subcloned

in pCR-Blunt as well. Both the untagged and the HA-tagged versions of the LDLRret

fragment were subsequently subcloned into the pcDNA3.1 Mammalian Expression Vector

(cat. V79020, Thermo Fisher Scientific) under the control of a CMV promoter. The coding

sequences of either construct were confirmed by Sanger sequencing. In the overexpression

experiments, HEK293T cells were seeded first in 6 wells plates, $1*10^6$ cells/well in complete

medium. 16 hours after seeding, 2.5 µg per well of pcDNA3.1 encoding for the LDLRret

fragment were transfected using Lipofectamine 3000 (cat. L3000015, Invitrogen) according to

the manufacturer's instructions (7 µL of Lipofectamine 3000 and 5 µL of P3000 reagent per

well). The same amount of an empty pcDNA3.1 vector was used as control. For proteasomal

inhibition studies, the cells were exposed to the MG-132 (cat. SML1135, Merck) proteasomal

inhibitor at a concentration of 5 µmol/L in DMSO as described previously[37]. Protein lysates and media were collected 48 h after transfection. Media were spun at 1500g for 5 minutes and the supernatant was used to detect the fragment.

Molecular cloning of *RBM25* and its mutants

The coding sequences of the wild type (wt) and the *RBM25* mutants were designed based on NCBI's reference sequence NM_021239.3 and were synthesized and cloned by Proteogenix (Schiltigheim, France) into pLVXpuro vector (cat. 632164, Takara Bio/ Clontech). The coding sequences of either construct were confirmed by Sanger sequencing. The coding sequences were thereafter subcloned into the pcDNA3.1 vector, by digesting the original pLVX-puro constructs with BstBI (cat. R0519S, NEB), Klenow (M0210S, NEB) and XbaI (cat. FD0685, Thermo Fisher scientific) and the pcDNA3.1 empty vector with EcoRV (cat. FD0303, Thermo Fisher scientific) and XbaI, respectively, according to the manufacturer's instructions. After gel purification with Zymoclean Gel DNA Recovery Kit (cat. D4001, Zymo Research), the digested material was ligated using T4 DNA ligase (cat. M0202S, NEB). The correct sequences of the generated plasmids were confirmed by both restriction enzyme digestion and Sanger Sequencing.

For the overexpression experiments, $4*10^5$ Huh-7 cells were seeded onto 6-well-plates. After 24 hours, the cells were transfected with 4 µg from each plasmid using Lipofectamine 2000 (cat. 11668019, Invitrogen) according to the manufacturer's instructions (6 µL lipofectamine 2,000/well). The same amount of empty pcDNA3.1 vector was used as the control. 24 hours after transfection the cells were treated with complete medium (DMEM containing 10% FBS) supplemented with 750 µg/mL G418 (cat. 10131-027, Gibco) for an additional 48 hours before being harvested.

Western blotting

Protein levels of LDLR and RBM25 in the whole cell lysate were determined by Western blotting 72 hours after transfection. Firstly, proteins were separated on an 8% SDS-PAGE gel and then transferred to an Amersham Hybond P 0.45 PVDF membrane (GE Healthcare Europe, Glattburg, Switzerland). All antibodies (see Major Resource Table) were diluted in a 0.01% PBST solution containing 5% skim milk. Primary antibodies were incubated overnight at 4°C. Secondary antibodies were incubated for 2 hours at room temperature. Detection was carried out using Thermofisher Scientific SuperSignal™ West Pico PLUS Chemiluminescent Substrate (cat. 34577, Thermo Fisher Scientific) on a Fusion FX (Vilber Lourmat, Marne-la-Vallée, France) imaging system. Densitometry was performed using either the Image Studio Lite software (LI-COR Biotechnology, Lincoln, NE, USA) (Figures 4C,4D) or ImageJ (https://imagej.nih.gov/ij/; figures S3c, S3e).

For Western blotting experiments involving cells overexpressing the LDLRret fragment, proteins were first separated on a 15% SDS-PAGE gel and then transferred to an Amersham Hybond P 0.45 PVDF membrane. The HA-tagged form of the fragment was detected with an HRP-conjugated anti-HA antibody (monoclonal Ha-HRP, clone HA-7, cat. H6533, Sigma-Aldrich). Beta actin (cat. SC-1616, Santa Cruz) was used as the loading control.

Flow cytometry based analysis of LDLR cell surface expression

LDLR cell surface levels were determined by flow cytometry on alive Huh-7 cells. 72 hours after transfection, the medium was aspirated and the cells were washed twice with PBS and detached using Accutase® (cat. A6964, Sigma-Aldrich) for 5 minutes at 37°C. The cells were then collected in complete medium and counted using a Beckman Coulter Z2 cell counter (Beckman Coulter, Nyon, Switzerland). After counting, the cells were washed in ice cold PBS and then incubated in Blocking buffer (PBS containing 0.5% BSA and 2% FBS) for 30 minutes on ice. After blocking, the cells were incubated with a primary anti-LDLR antibody

(Santa Cruz Biotechnology (figure 4D) or Progen Biotechnik (figures S3g, S10e and S11d); see Major Resources Table) diluted to a final concentration of 2 μg/mL in FACS buffer (PBS containing 0.5% BSA and 0.05% NaN_3) for 1 hour on ice. After washing twice with FACS buffer, the cells were incubated with either a chicken anti-Mouse IgG (H+L) Cross-Adsorbed AlexaFluor 488-conjugated Secondary Antibody (cat. A-21200, Thermo Fisher Scientific) diluted to a final concentration of 4 μg/mL in FACS buffer for 1 hour on ice in the dark (figure 4D) or anti-Mouse IgG (H+L) Cross-Adsorbed AlexaFluor 647-conjugated Secondary Antibody (cat. A-21236, Thermo Fisher Scientific) (figures S3g, S10e and S11d). Finally, the cells were washed twice with FACS buffer and re-suspended in ice cold FACS buffer for subsequent acquisition. In all cases, cells incubated with the secondary antibody were used as negative controls, while cells not incubated with any antibody were additionally used for the data shown in figure 4D. Prior acquisition, and in order to exclude signal originating from dead cells (figures S3g, S10e and S11d), the cells were incubated with Propidium Iodide (PI) (cat. 81845, Fluka) and FITC-Annexin V (cat. 640945, Biolegend, London, UK) at final concentrations of 1 μg/mL and 2 μg/mL, respectively. Sample acquisition was carried out on a BD LSR II Fortessa (BD-Biosciences, Allschwil, Switzerland) and using BD FACSDIVA™ software. During acquisition, signal from cell debris (and signal from dead cells for Figure 4D) was excluded by applying the forward size scatter versus the side size scatter gating (FSC-A / SSC-A). Thereafter, the doublets were also excluded through gating (FSC-A / FSC-H). Finally, for data shown in figures S3g, S10e and S11d, to exclude signal originating from the dead cells, the double negative cells for both FITC-Annexin V and PI were selected by gating (FITC-A / PI-A). To account for the spectral overlap of the different fluorophores used, unstained and single stained controls were acquired and analyzed using the compensation function of the FACSDIVA™ software. In all experiments, approximately 10^4 events per condition recorded at the final gate containing the population of alive cells were used for analysis. Data analysis was carried out using FlowJo version 10 (FlowJO LLC, Ashland, OR,

USA). The Median Fluorescence Intensity (MFI) of each population was used for comparisons between the different conditions.

Measurement of Atto655-LDL via flow cytometry

Huh-7 cells were incubated with Atto655-LDL to measure the LDL uptake. Briefly, 72 hours post-transfection, the cells were washed with PBS and they were incubated with 10 μg/mL Atto655-LDL contained in Assay Medium (DMEM supplemented with 0.2% BSA), in the absence or presence of 100x (1 mg/mL) non-labeled LDL at 37°C. After 2 hours, the cells were washed with PBS and detached using Accutase® solution (cat. A6964, Sigma Aldrich, Switzerland). Prior to acquisition, and in order to exclude signal originating from dead cells, the cells were incubated with PI and FITC-Annexin V, as described above. Sample acquisition was carried out on a BD LSR II Fortessa (BD-Biosciences, Allschwil, Switzerland) and using BD FACSDIVA™ software. During acquisition, the signals originating from cell debris and from doublets were excluded as described above. Finally, to exclude signal originating from the dead cells, the double negative cells for both FITC-Annexin V and PI were selected by gating (FITC-A /PI-A). To account for the spectral overlap of the different fluorophores used, unstained and single stained controls were acquired and analyzed using the compensation function of the FACSDIVA^{TM} software. In all experiments, approximately 10^4 events per condition recorded at the final gate containing the population of alive cells were used for analysis. Data analysis was carried out using FlowJo version 10 (FlowJO LLC, Ashland, OR, USA). Specific cellular uptake of LDL was calculated by subtracting the Median Fluorescence Intensity (MFI) value obtained for each sample in the presence of excess unlabeled LDL (unspecific) from the respective MFI value obtained in the absence of unlabeled LDL (total) of the respective sample.

Analysis of LDLR expression by targeted proteomics

To confirm LDLRret fragment overexpression by targeted proteomics, cell lysates from transfected HEK293T were first separated on a SDS-PAGE (4-12% Bis-Tris gel, Expedeon) and the bands corresponding to the full size LDLR protein and to the LDLRret fragment were excised and subjected to in-gel trypsin digestion[37]. Two peptides were used for quantification of the LDLR protein: peptide 1 (CIPQFWR) being located in the overlapping part of the protein and peptide 2 (NVVALDTEVASNR) representing a portion of LDLR that is specific for the full-length protein. Isotopically labeled standard peptides (CIPQFWR containing $^{13}C^{15}N$-labeled arginine, PEPotec grade 2 Thermo Scientific; NVVALDTEVASNR containing $^{13}C^{15}N$-labeled arginine derived from a synthetic protein concatemer, PolyQuant GmbH, Regensburg, Germany) were added to the trypsinized samples for relative comparison of the different samples. The peptides were targeted and analyzed by a triple quadrupole mass spectrometer (MS) equipped with a nano-electrospray ion source (TSQ Vantage, Thermo Scientific) coupled to liquid chromatography (Ultimate 3000 nano-UHPLC system, Dionex) as described previously[37]. The MS traces were manually curated using the Skyline software[38] and the summarized peak areas for the endogenous peptide and isotopically labeled standard peptides were plotted. The endogenous amount was estimated by reference to the known amount of the isotopically labelled standard peptides that was injected in the LC-MS measurement.

Minigene experiments

Both the short (chR19:11,102,285-11,102,921) and the long (chR19:11,102,283-11,105,702) *LDLR* genomic sequences of interest were amplified by PCR from HEK293T genomic DNA using the primer couples reported in Table S11, cloned first in pCR-Blunt and then subcloned in the pSPL3 exon trapping vector[39] for expression. Reaction conditions for PCR cloning of the short construct: Step 1: 95ºC, 2 minutes; Step 2: 95ºC, 30 seconds; Step 3: 66ºC, 30

seconds; Step 4: 72ºC, 70.0 seconds; Step 5: Repeat steps 2-4 29 more times; Step 6: 72ºC, 5 minutes; Step 7: 4ºC, until collection. Reaction conditions for PCR cloning of the long construct: Step 1: 95ºC, 2 minutes; Step 2: 95ºC, 30 seconds; Step 3: 66ºC, 30 seconds; Step 4: 72ºC, 6minutes; Step 5: Repeat steps 2-4 29 more times; Step 6: 72ºC, 5 minutes; Step 7: 4ºC, until collection.

To determine the splicing patterns of exons 3 and 4 in *LDLR*, the two *LDLR* minigenes as well as an empty pSPL3 vector were transfected in HEK293T cells according to the same protocol described above for the LDLRret fragment overexpression studies. 48 hours after transfection, the cells were lysed in Trizol Reagent (cat. 15596026, Thermo Fisher Scientific) and the lysates were used for total RNA extraction as described above. RNA sequencing on poly-A selected transcripts was performed as described above and sequencing reads were aligned to the reference sequence of each minigene construct. The coverage data shown in this manuscript were obtained from .bam files using the backbone of the long *LDLR* minigene as reference for alignment and were normalized to the average coverage in Exon 3 of *LDLR*.

Expression of spliceosome genes and *LDLR* transcripts in human liver

Healthy human liver tissue was obtained from 17 individuals undergoing partial hepatectomy because of either focal nodular hyperplasia or hepatocellular adenomas at the Academic Medical Center, University of Amsterdam, Amsterdam, The Netherlands. Spare normal tissue, defined as based on portal tract and central vein architecture, less than 5% steatosis, no inflammation, cholestasis and/or fibrosis, was used for RNA extraction and qRT-PCR analysis. Nine additional liver biopsies were obtained in the Division of Hepatology, University Hospital Würzburg, Germany from patients suspected to have NAFLD and were included into the qRT-PCR analysis as well.

Individual *LDLR* transcript expression was analysed in RNA Sequencing data of human liver samples obtained from 14 healthy individuals, 12 obese individuals without non-alcoholic

fatty liver disease (NAFLD), 15 patients with NAFLD, and 16 patients with non-alcoholic steatohepatitis (NASH) (Gene Expression Omnibus, accession number GSE126848)[8]. Upon a detailed examination of the quality of each sample, 1 sample of a healthy individual (SRR8601557) and 1 sample of a NASH patient (SRR8601555) were excluded from the generated plots due to lower quality of the reads. Although the sample SRR8601570 had 2-3x lower number of mapping reads compared to the rest of the samples, it was retained for analysis. Transcipts per million (TPM) and expected counts were computed using the RNA sequencing quantification software Salmon in quasi-mapping-based mode. The reference transcriptome used was ref. Ensembl 97, GRCh38.p12 (human).

Human liver biopsies were obtained at the Obesity Clinic of the Antwerp University Hospital from 155 non-diabetic, obese (BMI > 35) patients as described previously[9]. Briefly, patients suspected for NAFLD were biopsied at baseline and referred for intensive dietary intervention or bariatric surgery depending on presence of comorbidities. For gene expression analysis using the Affymetrix Human Gene 2.0 ST array, data was normalized by Robust Multichip Averaging (RMA) at the transcript level using the oligo package in R (R-project.org). To assess *LDLR* exon usage, RMA was applied at the probe level and each probe's intensity was normalized by the total *LDLR* expression for that patient as calculated by the transcript level summarization. Normalized probe intensities are presented as the $\log_2$ ratio of each probe to the total *LDLR* transcript expression in each patient.

LDLR transcript analysis in peripheral blood cells

Whole blood samples of 4,000 unrelated individuals were obtained from the Dutch BIOS consortium[10]. Paired-end RNA-sequencing data were generated. A reference sequence using the human genome build hg19 and Ensembl annotation version 75 was generated using the Kallisto[40] (v 0.42.2.1) index. Subsequently the paired-end fastq files were used as input for Kallisto quant, which was executed with the aforementioned reference sequence to quantify

transcript abundances per sample. For the *LDLR* transcript analysis, the available phenotype data were first filtered for missing values. After excluding samples of individuals without data on LDL cholesterol, 2,462 samples were left. A Spearman correlation test was performed between the TPM values normalized with Kallisto (see above) and the phenotypes of interest using the R cor.test function.

Analysis of the UK Biobank data

The raw GWAS data for variants and phenotypes were downloaded from

http://www.nealelab.is/uk-biobank (Version 2). The data included associations of 13,791,467 detected and imputed SNPs from 361,194 samples (194,174 females and 167,020 males) from the UK biobank. Regression models were adjusted for age, age^2, inferred_sex, age * inferred_sex, age^2 * inferred_sex, and principal components (PCs) 1 to 20. Variants were assigned to each gene by using the UCSC Genome Browser Variant Annotation Integrator (https://genome.ucsc.edu/cgi-bin/hgVai), build GRCh37/h19. Only variants between the transcription start and end were considered as shown in Table S12. P values for associations were corrected using the Bonferroni correction method based on the total number of variants (1360) in the selected genes. Association between exome variants in the elected genes were downloaded from the Amazon cloud server s3://helix-researchpublic/ukbb_exome_analysis_results/V1.3/, as provided by Helix Research and UK Biobank[11,41]. The latest version of the analysis (1.3) was used. Data included 984,819 variants in 15,474 genes from 40,468 exomes. Both loss of function and coding-based models were considered for European and all ethnicities. Data analysis and visualization was done using R (R-project.org).

Associations of the *RBM25* SNP rs17570658

The association of the lead SNP in *RBM25* rs17570658 with LDL cholesterol was meta-analysed according to METAL[14] using data of eight studies with 435,884 subjects summarized by the CardioVascular Disease Knowledge Portal (https://cvd.hugeamp.org/variant.html?variant=rs17570658) plus data of 19,653 participants of the Copenhagen City Heart Study and the Copenhagen General Population Studies genotyped with exome chip arrays[13]. The association of rs17570658 with *RBM25* gene expression was analysed by using data of nearly 1000 individuals collected by the Genotype-Tissue Expression (GTEx) project (GTeX https://gtexportal.org/home/). Nominal p values for each variant–gene pair were estimated using a two-tailed t-test. The significance of the most highly associated variant per gene was determined from empirical P values, extrapolated from a Beta distribution fitted to adaptive permutations with the setting –permute 1000 10000. These empirical p-values were subsequently corrected for multiple testing across genes using Storey's q value method[26,27].

Analysis of *RBM25* gene variants in FH patients

Whole exome sequencing (WES) data of 71 FH probands negative for mutations in the known major FH-causing genes (*LDLR*, *APOB*, and *PCSK9*) were generated as part of the UK10K project[15]. A previous analysis suggested an enrichment of rare (minor allele frequency [MAF] $< 5.0 * 10^{-3}$) *RBM25* gene variants in the FH cohort in comparison to 1926 controls from the UK10K study[15]. The gene burden test was re-analyzed by applying binomial test to a much larger control cohort of 56,352 European data provided by the gnomAD study[12]. Variants identified by WES in both FH cases and gnomAD, were filtered to select those with MAF$< 1.0 * 10^{-4}$ that were annotated as missense or loss of function. The MAF cut-off of $1.0 * 10^{-4}$ was based on the analysis of another genetically heterogeneous dominant disease, hypertrophic cardiomyopathy, as previously demonstrated by Whiffin et al[42].

Statistics

The RNAi screening assay feature data were analyzed as follows: data were first normalized by the median value of each batch, microscope, plate and well and were finally expressed as robust Z-score[43] normalized values. The Redundant siRNA Activity (RSA) analysis was performed for each assay feature on the normalized data to rank the genes and detect the top hits[44], defined here as the genes with an RSA p value of less than 0.001. This p value cutoff was dictated by our ability to verify the results *in vitro*.

Transfection efficiency and the dynamic range of the screening assay were determined by calculating the Z'-factor between positive and negative transfection and assay controls as published before[43]. Dimensionality reduction across the five main assay features mentioned above was performed using the Locally-Linear-Embedding[45] method on $\log_2$-transformed data through the *sklearn* Python implementation of the method (http://scikit-learn.org/).

Top hits were clustered by function using the online String tool (https://string-db.org/), version 11.0 according to the following settings: the network edges indicate the type of interaction evidence, all active interaction sources (textmining, experiments, databases, co-expression, neighbourhood, gene fusion, co-occurrence) were selected for the analysis, with the minimum interaction score set to 0.400 (medium confidence) and with no network clustering used. Gene Ontology (GO) analysis for statistical overrepresentation of GO-Slim biological process terms was performed using the Panther Gene List Analysis tool (http://www.pantherdb.org). Enrichment was calculated by Fisher's exact test and corroborated by the calculation of the false discovery rate (FDR) according to the Benjamini-Hochberg procedure. GO terms with FDR <0.05 were reported as significant in this manuscript.

Due to low numbers of replicate experiments, non-parametric tests of the GraphPad Prism version 8 were used to analyse the data of the validation experiments, namely Kruskal-Wallis test with either Dunn's multiple comparisons test for the experiments shown in figures 1C,

4C, 4D, and in figures S2b-d and S11 or. For one to one comparisons, the Mann-Whitney test (one-tailed) was used for the experiments shown in figure 1D and in figures S3, S5c and S10 or the Wilcoxon test (two-tailed) for the data shown in figures S8f and S8g. Correlations presented in figures 2C, 6, and S8a-e as well as tables S5 and S6 were calculated according to Spearman (two-tailed)Other statistical tests applied to the analysis of genetic data on RBM25 in data banks have been described before in the respective paragraphs. The p values presented in figures 5B, 5C, 6, 7A, S8, and S9a as well as tables S5 and S6 were adjusted for multiple testing according to the Bonferroni correction. Empirical p values shown in Figure 7B were corrected for multiple testing across genes using Storey's q value method[26,27].

The specific statistical tests and the adjustments for multiple testing used are also described in the legends of the respective figures and tables. P values, coefficients of correlation as well as regression equations are presented within the figures and tables.

Study approval

Human studies were approved by institutional boards of each institution involved: the ethics committee of the University Medical Centre Groningen, the Ethical Committee of the Antwerp University Hospital (file 6/25/125) and the Ethics Committee of the University Hospital Würzburg (AZ188/17 and AZ96/12). For the AMC liver samples, the local medical ethics committee "Medisch Ethische Toetsings Commissie van het Amsterdam UMC, locatie AMC" approved the protocol for this study before the General Data Protection Regulation (GDPR) law came into force, waiving the need of inform consent as the study employed spare biological material from hepatectomies with therapeutic purpose.

For the UK10K FH sequencing data, all consents and local review board approvals were in accordance with the UK10K project ethical framework. All participants provided written informed consent.

2. <u>Supplemental Figures</u>
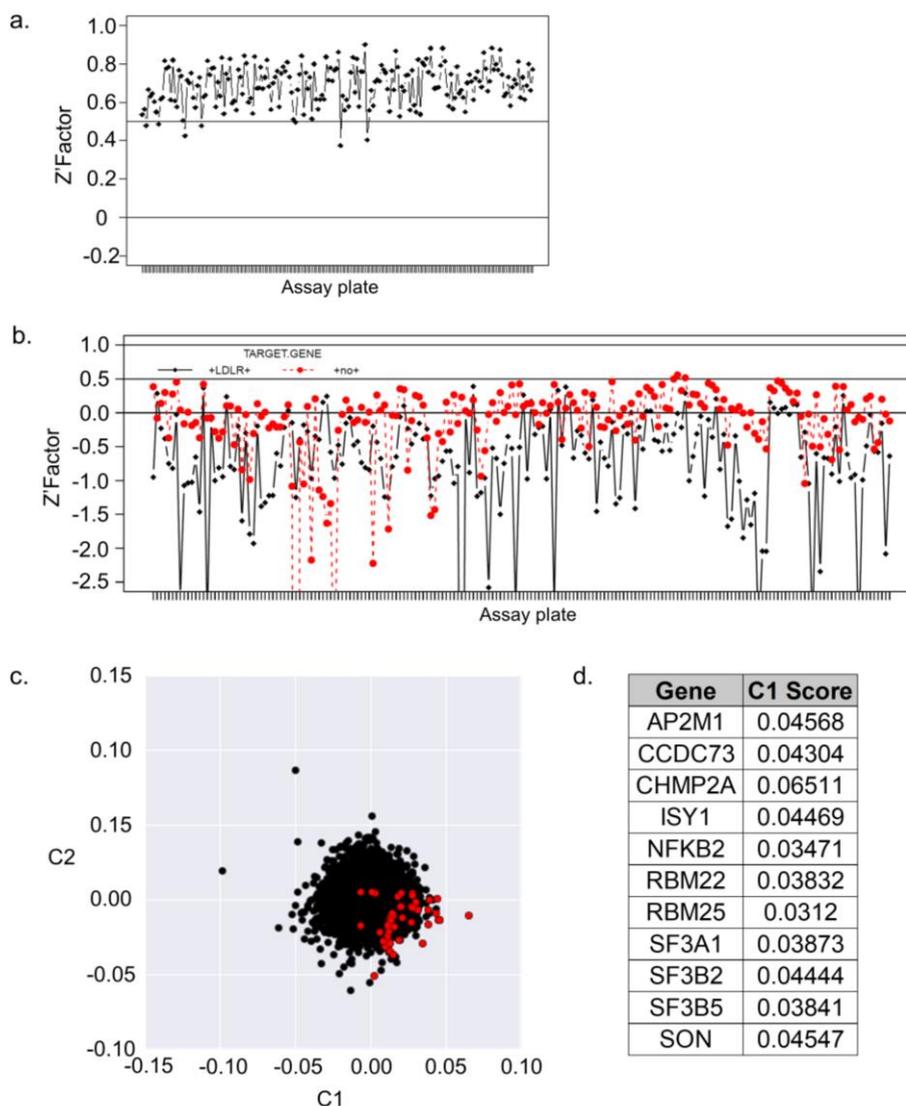
Figure S1. Quality control (QC) of the screening and non-linear dimensionality reduction of the dataset. a). QC for transfection efficiency. The effect size on nuclei counts of an siRNA against *PLK1*, an essential kinase that upon knockdown results in cell death, was measured in comparison to control wells that received a non-targeting siRNA pool and is expressed here as Z'-factor. Each dot represents one of the 192 screening plates. Z'-factors between 0.5 and 1 are considered excellent. **b). Overview on negative and positive controls.** This figure depicts the Z'-factors for median cytoplasm intensity in the LDL channel for negative control wells that did not receive any fl-LDL (in red) as well as for positive control wells that received an siRNA against *LDLR* (black). For either control, the Z'-factor was calculated in comparison to wells that received a non-targeting control siRNA and were subsequently incubated with fl-LDL. Z'-factors between 0.5 and 1 are considered excellent. **c). Locally linear embedding (LLE) analysis.** The graph shows the first two components of the screening dataset after LLE dimensionality reduction was applied. As LLE generates slightly different results at each iteration, a representative LLE outcome is reported in this figure. Each dot represents one gene. Red dots represent our top hit genes limiting LDL uptake after RSA analysis of the median cytoplasm intensity feature. Note how most of the red dots map at the extreme right of the C1 component. **d). Top hit genes after LLE.** This list contains all genes with a value over 0.03 on the C1 axis after LLE and corresponds to the iteration of the analysis shown on the left.
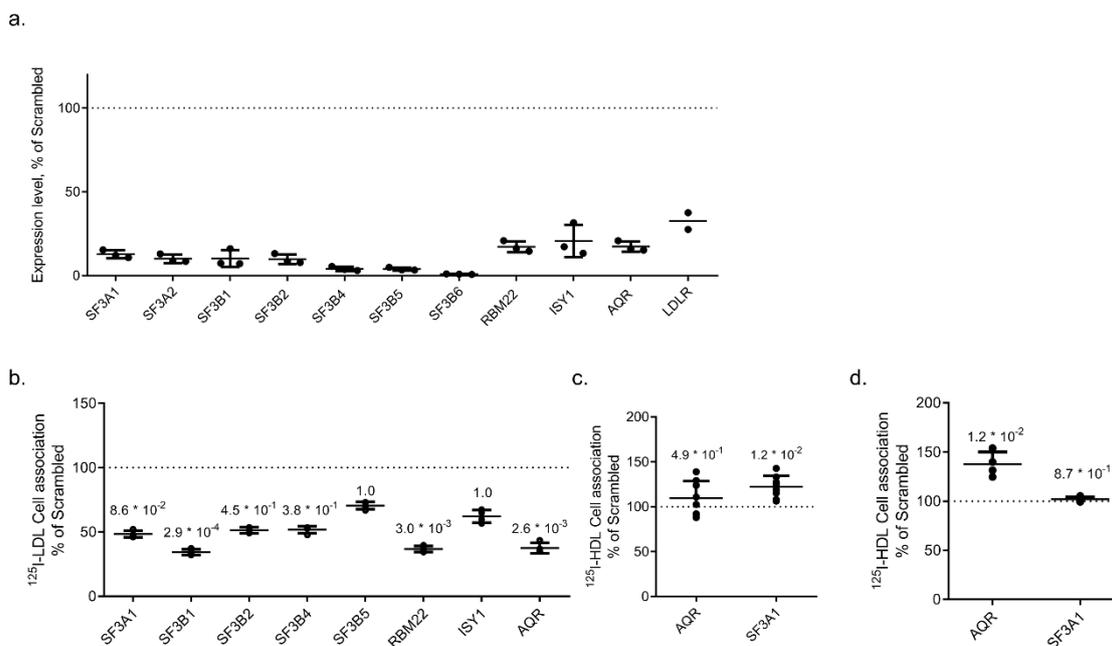
Figure S2. Additional *in vitro* validation experiments and determination of knockdown efficiency. a) Knockdown efficiency of siRNA pools in Huh-7 cells was measured by real-time PCR 72 hours after siRNA transfection and is expressed as percentage of expression compared to a non-targeting control (scrambled). With the exception of *LDLR* (from Ambion Silencer Select) all siRNAs were ON-TARGETplus Smart Pool siRNAs from Dharmacon. Data are shown as means±SD. **b) ^{125}I-LDL cell association in HepG2 cells. c) ^{125}I-HDL cell association in Huh-7 cells. d) ^{125}I-HDL cell association in HepG2 cells.** Cell association experiments were performed 72 hours after transfection with pooled siRNAs by incubating the cells for 2 hours at 37°C in the presence of 33.3 µg/ml of radioiodinated lipoproteins or 40 fold excess of the respective unlabeled lipoprotein. Data are means±SD of 3 triplicate experiments (**a**), 1 quadriplicate experiment (**b,d**), or 2 quadriplicate experiments (**c**). Statistical analysis (**b-d**) was performed using Kruskal-Wallis test with Dunn's multiple comparisons test between the non-targeting and each targeting siRNA; the respective p values are shown above each condition.
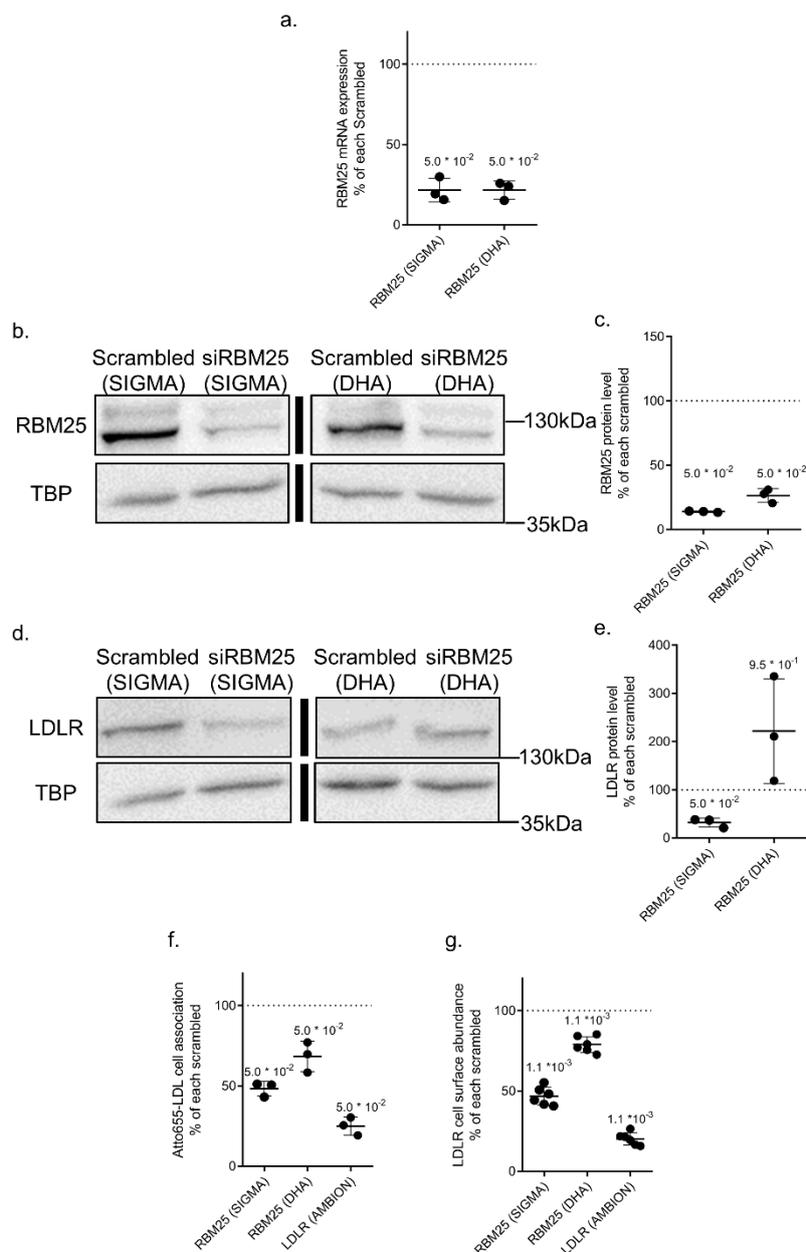
Figure S3. Validation of RBM25. a). Knockdown efficiency of siRNAs obtained from different vendors (Sigma or Dharmacon) in Huh-7 cells was measured by real-time PCR 72 hours after siRNA transfection and is expressed as percentage of expression compared to the respective vendor's non-targeting control (scrambled). Data are shown as means ±SD of 3 independent experiments. **b) and c) Effect of *RBM25* knockdown on RBM25 protein levels.** RBM25 protein levels in Huh-7 cells 72 hours after transfection with the indicated siRNAs were measured by western blot. A representative blot is shown in **b). c)** shows the relative density of RBM25 bands after knockdown of *RBM25* with the indicated siRNAs, relative to the respective non-targeting (scrambled) control. TATA-binding-protein (TBP) was used as the loading control. Data are shown as means ±SD of 3 independent experiments. **d) and e). Effect of *RBM25* knockdown on LDLR protein levels.** LDLR protein levels in Huh-7 cells 72 hours after transfection with the indicated siRNAs were measured by western blot. A representative blot is shown in **d). e)** shows the relative density of LDLR bands after

knockdown of *RBM25* with the indicated siRNAs, relative to the respective non-targeting (scrambled) control. TATA-binding-protein (TBP) was used as the loading control. Data are shown as means ±SD of 3 independent experiments. **f) Effect of *RBM25* knockdown on Atto655-LDL uptake**. Atto655-LDL uptake was measured 72 hours after transfection with siRNAs against *RBM25* or non targeting controls (scrambled) obtained from different vendors by incubating the cells for 2 hours at 37°C with 10 μg/ml Atto655-LDL in the presence or absence of 100-fold excess of unlabeled LDL. Data are shown as means ±SD of 3 independent experiments. **g) Effect of *RBM25* knockdown on LDLR cell surface levels**. LDLR cell surface levels in alive Huh-7 cells were measured by flow cytometry 72 hours after knockdown of RBM25 with the indicated siRNAs. The siRNA against *LDLR* was used as the positive control. The data are normalized to the respective vendor's non-targeting control. Data are shown as means ±SD of 6 independent experiments. In all cases, statistical analysis was performed using Mann-Whitney test (one-tailed) between each targeting siRNA and the respective non-targeting control (scrambled) of each vendor. The respective p values are shown above each condition.
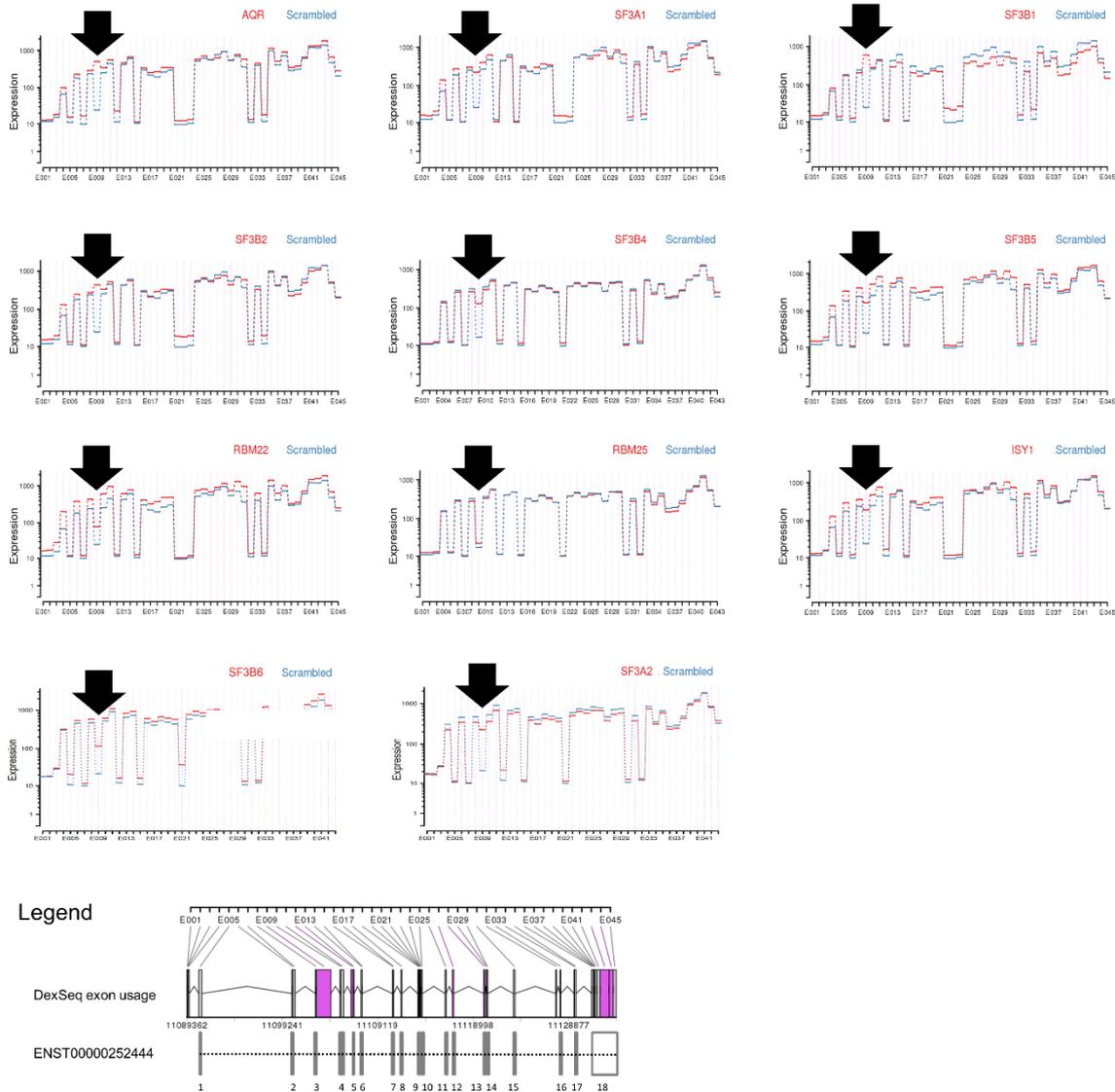
Figure S4. *LDLR* exon level expression after knockdown of U2-spliceosome genes. Expression of the *LDLR* exons was recorded by RNA sequencing of Huh-7 cells 72 hours after knockdown of each U2-spliceosome hit gene. Segments represent differential exon usage in each sector of the *LDLR* genomic sequence as identified by the DEXSeq algorithm and as summarized in the linear representation below the graph. Canonical exons belonging to the ENST00000252444 full-length transcript are depicted in the legend. Normalized read counts are reported on the y axis. The black arrow indicates the location of ENSG00000130164:E009, corresponding to the first half of intron 3. Data represent the average of 3 independent experiments.
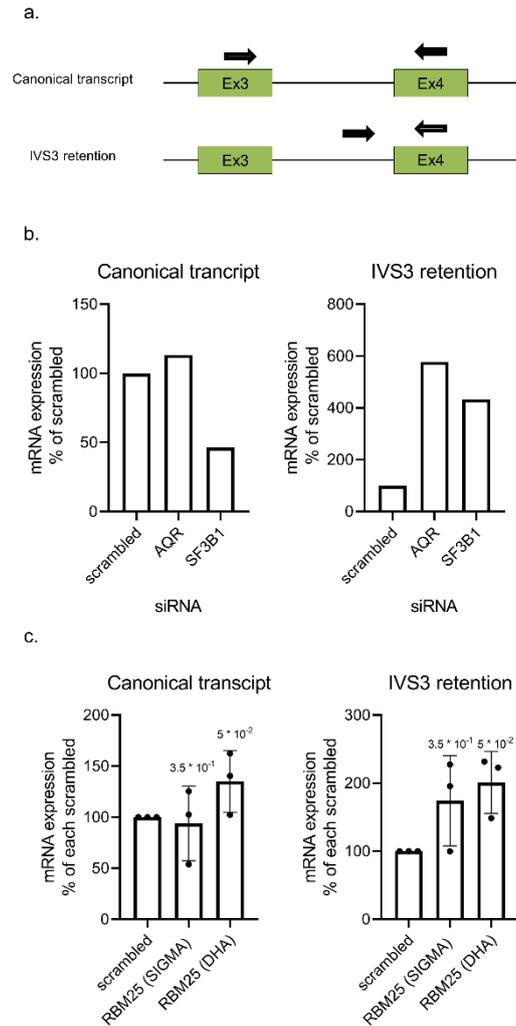
Figure S5. Confirmation of *LDLR* intron 3 retention by qRT-PCR. a). qRT-PCR setup. The approximate location of each primer within the region of *LDLR* spanning from exon 3 (Ex 3) to exon 4 (Ex 4) region is represented by black arrows. Primers are from Cameron et al.,[5]. IVS3 = intron 3. **b) and c) Expression levels of the full length and intron 3-retaining *LDLR* transcripts after knockdown of *AQR*, *SF3B1* (b) or *RBM25* (c) in Huh-7 cells.** Data are normalized to the respective non-targeting siRNA condition (scrambled) and are expressed as means of 1 triplicate experiment (**b**) or means±SD of 3 triplicate experiments (**c**). Statistical analysis in (**c**) was performed using Mann-Whitney test (one-tailed) by comparing each targeting siRNA with the respective non-targeting control (scrambled) of each vendor. The respective p values are shown above each condition.
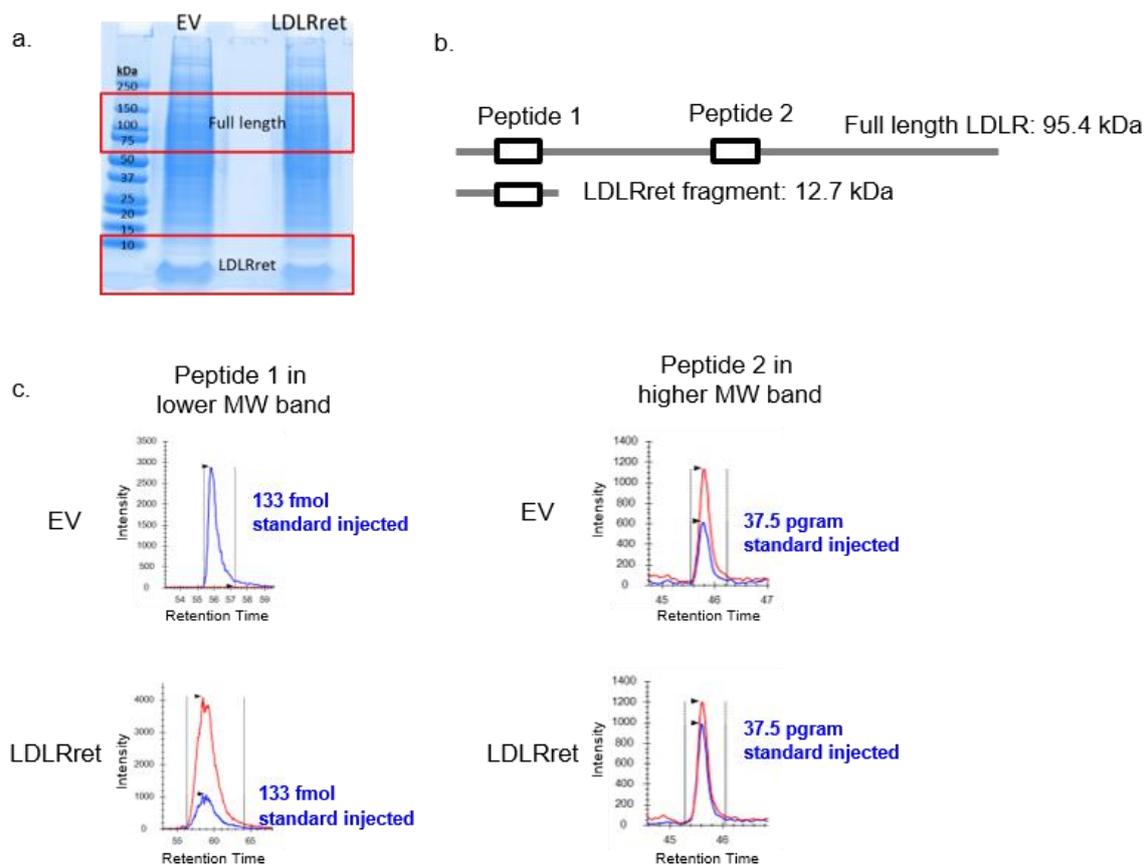
Figure S6. Detection of the LDLRret fragment by liquid-chromatography coupled mass spectrometry (LC-MS). The full length LDLR and fragment LDLR were separated on a SDS-PAGE (**a**) and the bands containing the full size protein and the LDLR fragment were excised and trypsinized with in-gel digestion. **b) Localization of the two LDLR peptides recorded by LC-MS:** peptide 1 is located in the overlapping part of the protein (but the fragment and full protein are already separated in the SDS-PAGE gel). Peptide 2 is specific for the full-length protein. Isotopically labeled standard peptides were added to the trypsinized samples for comparison of the different samples. **c) Quantification of endogenous LDLR peptides and isotopic standard peptides by LC-MS.** The peaks of the isotopically labeled standards are shown in blue, with the concentration of each standard depicted next to it. The peaks of the endogenous peptides are shown in red and the peak boundaries are annotated with black dotted lines. These analyses were done for three types of samples: a sample with the LDLR fragment being overexpressed (untagged) annotated as LDLRret, an empty vector control annotated as EV and detection in a plasma pool (not shown).

a.

b.

c.

d.

e.
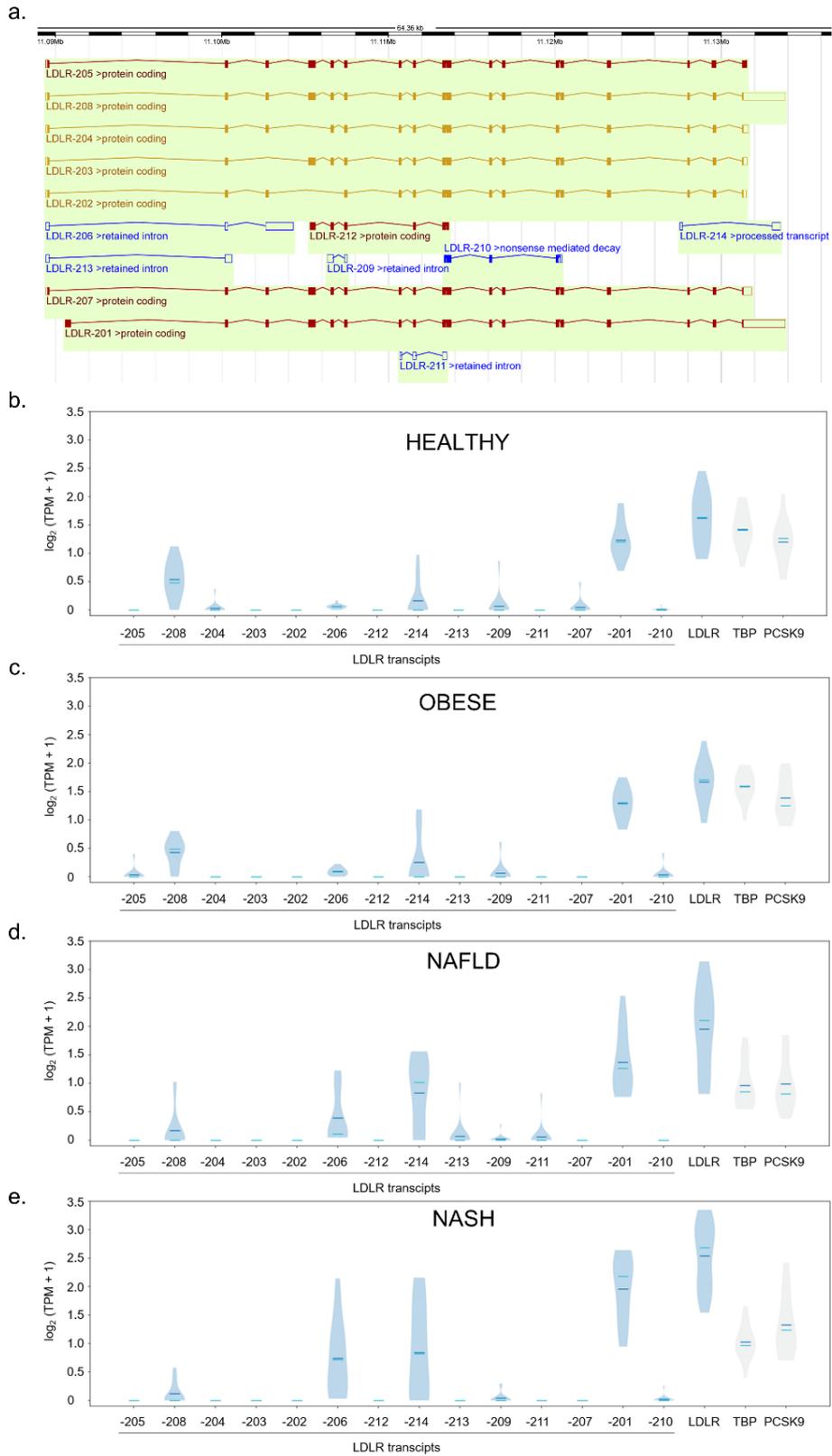
Figure S7. Quantification of different *LDLR* transcripts expressed in livers of individuals without or with non-alcoholic fatty liver disease (NAFLD) by RNA sequencing. a). Illustration of the different *LDLR* transcripts. The different *LDLR* transcripts and the exons/introns included for each transcript were retrieved and adapted from ensemble's webpage: https://www.ensembl.org/Homo_sapiens/Gene/Summary?db=core;g=ENSG00000130164;r=19:11089462-11133820. **b-e). Interindividual and disease-dependent variation of LDLR transcript expression in human liver**. Computational analysis of previously published RNA sequencing data of liver samples from 13 non-obese (**b**) and 12 obese individuals without NAFLD (**c**) as well as 15 patients with NAFLD, and 15 patients with non-alcoholic steatohepatitis (NASH, **d**). (Gene Expression Omnibus, accession number GSE126848)[8]. Graph depicts the $\log_2$ transcript per million (TPM) levels (y-axis) for each of the annotated *LDLR* transcripts, the sum of all 13 *LDLR* transcripts, and the reference genes *TBP* and *PCSK9* (x axis). The dark blue and the light blue lines within each violin correspond to the mean and median values, respectively.
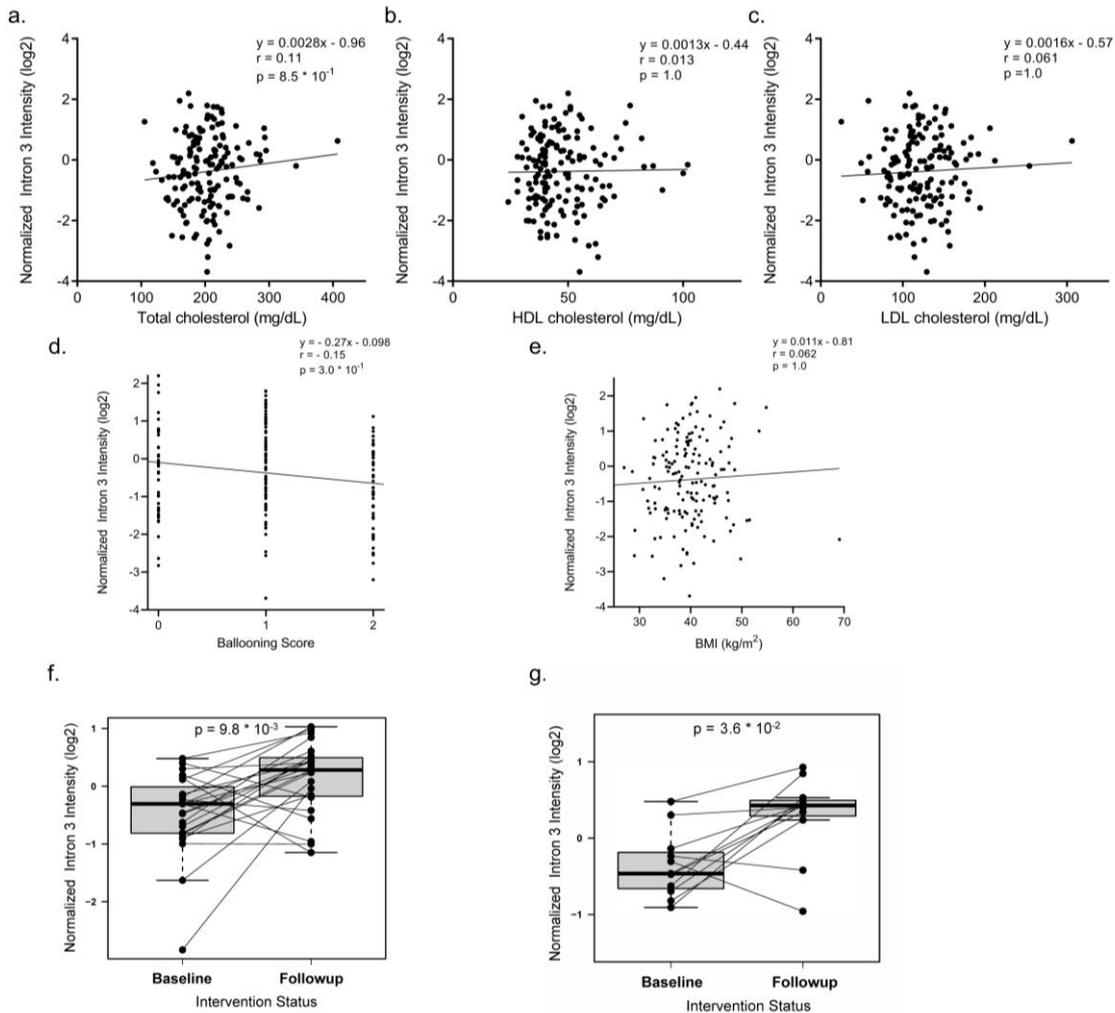
Figure S8. Hepatic expression of *LDLR* Intron 3 retention does not correlate with plasma lipids but increases upon bariatric surgery in obese subjects[9]. **a-e.** Hepatic Intron 3 probe intensity is shown after $\log_2$ transformation. **Correlations of intron 3 probe relative intensity values with plasma levels of total (a), HDL- (b) and LDL- cholesterol (c), histological ballooning score (d)**, **or BMI (e) in the entire cohort at baseline (n = 155).** Regression equations, Spearman coefficients of correlation (r) as well as p values adjusted for multiple testing according to Bonferroni correction are reported for each graph **f)** and **g). Effect of bariatric surgery on intron 3 retention.** Intron 3 retention levels for patients from whom hepatic mRNA was available at baseline and after bariatric surgery (median follow-up time 13 months, IQR = [12 months, 15 months]). Data from all 21 paired biopsies (**f**) and from 11 paired biopsies of responders (**g**), defined as having non-alcoholic steatohepatitis (NASH) at baseline but no NASH at follow-up. Normalized intron 3 is calculated as the ratio between Robust Multichip Averaging (RMA)-normalized probe intensity for the intron 3 probe and the RMA-normalized total *LDLR* transcript level for each sample. The diagonal lines connect the datapoints of each individual. The p values reported were calculated using the Wilcoxon matched-pairs signed rank test and were adjusted for multiple testing according to Bonferroni correction.
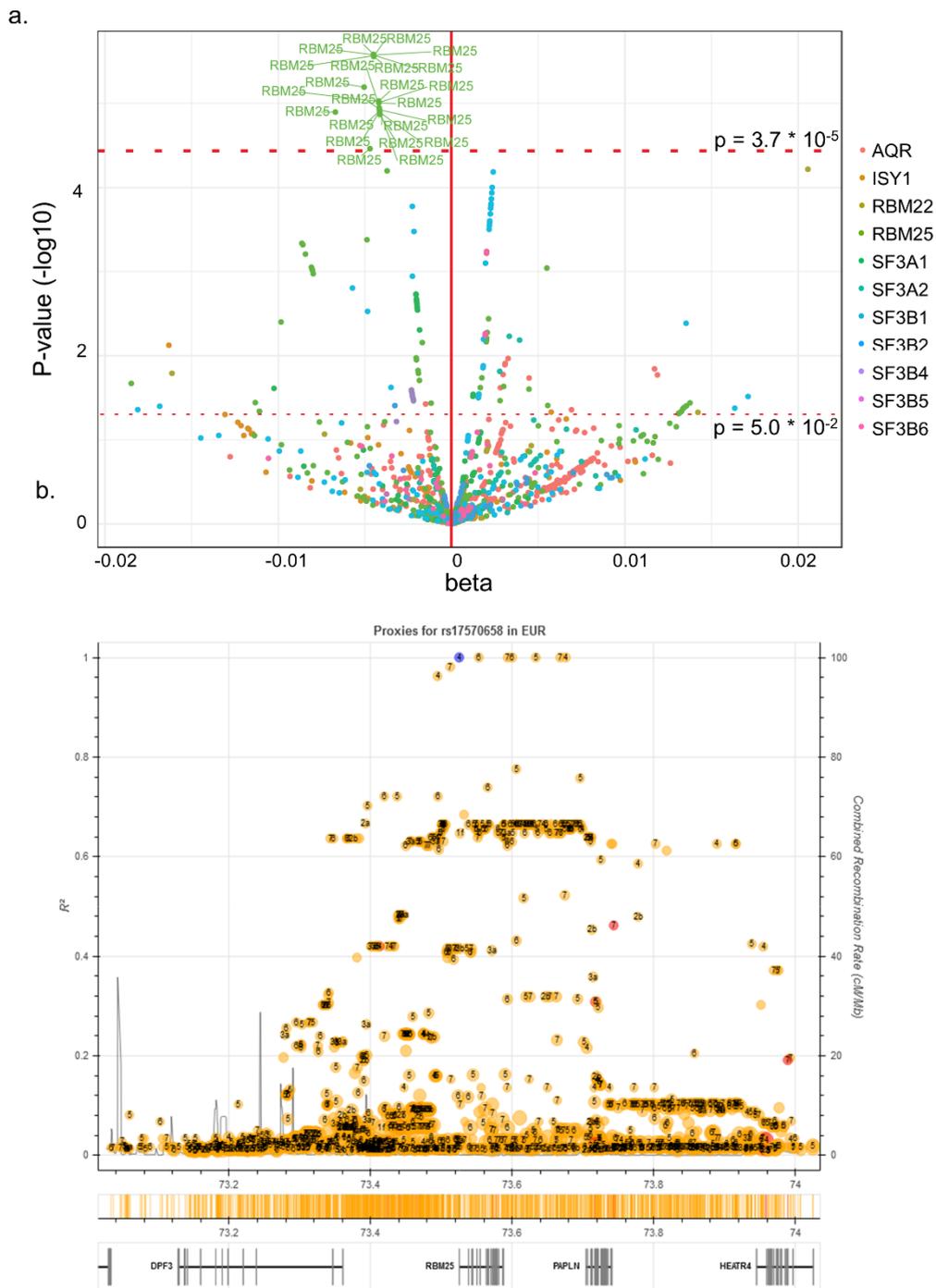
Figure S9. a). Association between RBM25 variants and plasma apoB levels in the UK Biobank dataset. The dashed red horizontal lines indicate the p=0.05 threshold as well as the threshold for statistical significance after Bonferrroni correction for multiple testing of 1360 variants within the genes of interest (p=3.7*10^{-5}), respectively. Effect size and directionality are reported on the x axis as beta value. **b). Linkage disequilibrium information for the rs17570658 SNP in Europeans.** Data from Phase 3 (Version 5) of the 1000 Genomes Project were plotted using the LDproxy tool at LDlink (https://ldlink.nci.nih.gov/) and are expressed as R2. rs17570658 is indicated by the blue circle

a.

RBM25

b.

Canonical Transcript

c.

IVS3 retention

d.

e.
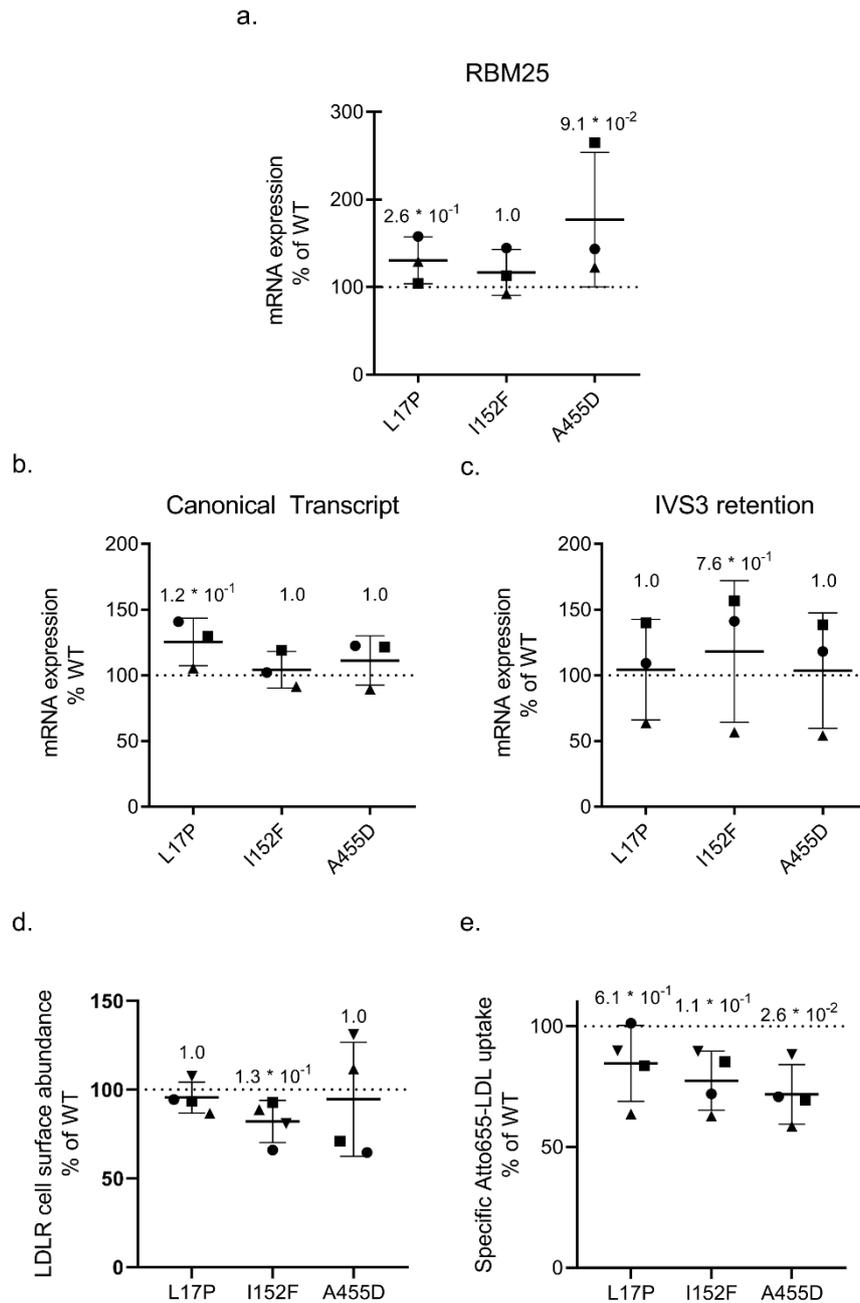
Figure S11. Impaired LDL uptake by Huh-7 cells overexpressing RBM25 mutants. 72 hours after plasmid transfection and 48 hours after introduction of the selection antibiotic G418, the cells were harvested and analyzed by using RT-PCR (**a, b, c**) and flow cytometry (**d, e**). Overexpression of wild type and mutant RBM25 constructs cause comparable increases in mRNA levels of *RBM25* (**a**), *LDLR* canonical transcript (**b**) and IVS3 transcript (**c**). **d)** LDLR cell surface abundance is not altered upon expression of RBM25 mutants compared to wild type RBM25. **e)** Uptake of fluorescently labeled LDL is lower in cells overexpressing RBM25 mutants than in cells overexpressing wild type RBM25. In all graphs, data are normalized to wild type RBM25 (WT) and are shown as means ±SD, with each dot representing 1 of 3 independent (**a-c**) or 4 independent (**d, e**) experiments. Numbers in the graphs are p values calculated by Kruskal-Wallis test with Dunn's multiple comparisons test by comparing WT with each mutant.

3. Supplemental Tables

Table S1 (Provided as Excel file). Complete screening dataset for the five best performing assay features. The assay features values are normalized as reported in the methods section. Non self-explanatory column names are as follows: Gene.ID.20160314: NCBI Gene-ID on 2016.03.14; siRNA.ID: siRNA molecule ID as according to manufacturer; Gene.Symbol.20160314: NCBI Gene Symbol on 2016.03.14; RefSeq.Accession.Number: NCBI RefSeq ID for the targeted transcript; Batch: experimental batch number; FL.LABEL: describes whether the well received fluorescently-labeled LDL; RNASeq_Huh-72..Signal.: normalized gene-level expression as measured by RNA sequencing; RNASeq_Huh-72..Present.: dichotomic gene-level expression label (threshold 7.5). For each assay feature, RSA p values are given for both directionalities of the RSA analysis (inhibition and enhancement of LDL uptake). No RSA p values were generated for empty wells, control wells, wells without an associated Gene.ID as well as wells that did not meet the lower ranking threshold for the RSA analysis.

Table S2. Results of the Panther GO-Slim BP enrichment test.

PANTHER GO-Slim Biological Process	RL	HG	EV	FE	p	FDR
intra-Golgi vesicle-mediated transport (GO:0006891)	28	3	0.07	40.9	$7.20*10^{-05}$	$7.61*10^{-3}$
mRNA splicing, via spliceosome (GO:0000398)	164	7	0.43	16.29	$3.02*10^{-7}$	$2.71*10^{-4}$
macromolecule metabolic process (GO:0043170)	2419	22	6.34	3.47	$6.73*10^{-8}$	$1.21*10^{-4}$
organic substance metabolic process (GO:0071704)	3338	22	8.74	2.52	$1.62*10^{-5}$	$2.08*10^{-3}$
metabolic process (GO:0008152)	4072	22	10.67	2.06	$4.42*10^{-4}$	$4.18*10^{-2}$
RNA processing (GO:0006396)	233	7	0.61	11.47	$2.92*10^{-6}$	$4.04*10^{-4}$
gene expression (GO:0010467)	1842	14	4.83	2.9	$2.23*10^{-4}$	$2.23*10^{-2}$
RNA splicing, via transesterification reactions with bulged adenosine as nucleophile (GO:0000377)	164	7	0.43	16.29	$3.02*10^{-7}$	$1.81*10^{-4}$
RNA splicing, via transesterification reactions (GO:0000375)	165	7	0.43	16.2	$3.14*10^{-7}$	$1.41*10^{-4}$
RNA splicing (GO:0008380)	176	7	0.46	15.18	$4.77*10^{-7}$	$1.22*10^{-4}$

Table S2 (continued). Results of the Panther GO-Slim BP enrichment test.

PANTHER GO-Slim Biological Process	RL	HG	EV	FE	p	FDR
proteasome-mediated ubiquitin-dependent protein catabolic process (GO:0043161)	142	5	0.37	13.44	$4.07*10^{-5}$	$4.88*10^{-3}$
macromolecule catabolic process (GO:0009057)	300	8	0.79	10.18	$1.29*10^{-6}$	$2.31*10^{-4}$
proteolysis involved in cellular protein catabolic process (GO:0051603)	253	8	0.66	12.07	$3.69*10^{-7}$	$1.33*10^{-4}$
cellular protein catabolic process (GO:0044257)	255	8	0.67	11.98	$3.91*10^{-7}$	$1.17*10^{-4}$
protein catabolic process (GO:0030163)	289	8	0.76	10.57	$9.79*10^{-7}$	$2.20*10^{-4}$
proteasomal protein catabolic process (GO:0010498)	153	5	0.4	12.48	$5.75*10^{-5}$	$6.45*10^{-3}$
protein ubiquitination (GO:0016567)	200	7	0.52	13.36	$1.09*10^{-6}$	$2.18*10^{-4}$
protein modification by small protein conjugation (GO:0032446)	217	7	0.57	12.31	$1.85*10^{-6}$	$2.77*10^{-4}$
protein modification by small protein conjugation or removal (GO:0070647)	217	7	0.57	12.31	$1.85*10^{-6}$	$3.02*10^{-4}$

Only categories with FDR<0.05 are displayed. The categories are sorted by the Fold Enrichment of the most specific categories (highlighted in bold), with their parent terms (p-value lower than 0.05) indented directly below. RL: Reflist genes, number of genes in the Panther reference list that map to each particular GO-Slim BP category; HG: hit genes, number of screening hit genes that map to each category; EV: expected value, expected number of genes mapping to each category if no enrichment were present; FE: Fold enrichment, FE is calculated as the ratio between the number of hit genes detected by the screen and the expected value. p: raw p values based on a Fischer's exact test; FDR: False discovery rate

Table S3. *In silico* **BPS predictions in human and mouse.**

Species	agez	ss_dist	bp_seq	bp_scr	y_cont	ppt_off	ppt_len	ppt_scr	svm_scr
human	43	294	tactcaacc	0.80074	0.50519	35	12	16	-1.18792
human	43	283	aaataagga	-2.45889	0.51079	24	12	16	-1.76613
human	43	266	ctataaatt	-1.48048	0.51724	7	12	16	-0.30488
human	43	240	gtctcagtt	0.00264	0.50638	10	13	20	0.11969
human	43	235	agtttaaca	-3.81564	0.50435	5	13	20	-1.05951
human	43	234	gtttaacag	0.47649	0.50655	4	13	20	0.68507
human	43	226	gctttacac	-1.87418	0.50226	103	22	33	-6.38214
human	43	217	ctattagcg	-2.00591	0.49528	94	22	33	-5.86629
human	43	202	tgctcatag	0.87151	0.49239	79	22	33	-3.7911
human	43	173	agatgagga	-3.29087	0.51786	50	22	33	-3.57699
human	43	164	aactgaggc	0.04083	0.53459	41	22	33	-1.69739
human	43	141	ggttcagag	-1.70368	0.56618	18	22	33	-0.91438
human	43	124	ccctgactg	3.62683	0.57143	1	22	33	2.25053
human	43	87	gcctcactg	1.97921	0.52439	70	13	21	-2.88916
human	43	38	acttcacac	-0.61163	0.60606	21	13	21	-0.7756
human	**43**	**30**	**cggtgatgg**	**1.7613**	**0.68**	**13**	**13**	**21**	**0.68379**
mouse	29	295	gtataattt	-0.89117	0.4931	63	10	13	-4.07236
mouse	29	291	aatttatac	-3.30713	0.48951	59	10	13	-4.70549
mouse	29	283	catttagca	-2.73307	0.48561	51	10	13	-3.8971
mouse	29	274	agataagca	-1.35831	0.49442	42	10	13	-2.70381
mouse	29	253	acctaaagc	0.36538	0.49597	21	10	13	-0.49484
mouse	29	246	gcattaaga	-3.75146	0.49793	14	10	13	-1.55753

Table S3 (continued). *In silico* **BPS predictions in human and mouse.**

Species	agez	ss_dist	bp_seq	bp_scr	y_cont	ppt_off	ppt_len	ppt_scr	svm_scr
mouse	29	245	cattaagat	-0.94489	0.5	13	10	13	-0.40666
mouse	29	234	ggctcaata	-0.62438	0.50218	2	10	13	0.52747
mouse	29	218	cagtgaggg	-1.10555	0.49765	98	11	12	-6.73381
mouse	29	210	ggctcatag	0.16255	0.50244	90	11	12	-5.65641
mouse	29	190	gcttgatag	-0.89592	0.51351	70	11	12	-4.58519
mouse	29	183	agttgacca	1.31323	0.51685	63	11	12	-3.22098
mouse	29	171	ggatgagga	-2.5864	0.5241	51	11	12	-3.83023
mouse	29	132	tcctgagcc	1.0425	0.5748	12	11	12	0.45168
mouse	29	99	tgctaaatg	1.46063	0.56383	6	12	21	1.06719
mouse	29	80	ttttgaagc	-1.06802	0.57333	10	10	16	-0.20359
mouse	29	45	gtgtaagcc	-0.29433	0.675	18	15	31	-0.43572
mouse	**29**	**33**	**gcctgacag**	**2.01588**	**0.75**	**6**	**15**	**31**	**1.35885**

Each entry represents a putative U2-dependent branch point identified by the SVM-BP-finder algorithm. Results for the last 300nt of each intron are displayed. A BPS is considered valid when located close to the AG exclusion zone (AGEZ; the distance to 3'ss is usually approx. within AGEZ + 9nt), with BP-score > 0 and with svm_score > 0. The two entries matching these requirements in man and in mouse are highlighted in bold and underlined. agez: AG dinucleotide Exclusion Zone length; ss_dist: Distance to 3' splice site; bp_seq: BP sequence (nonamer; from -5 to +3 relative to the BP adenine); bp_scr: BP sequence score using a variable order Markov model; y_cont: Pyrimidine content between the BP adenine and the 3' splice site; ppt_off: Polypyrimidine tract offset relative to the BP adenine; ppt_len: Polypyrimidine tract length; ppt_scr: Polypyrimidine tract score; svm_scr: Final BP score using the SVM classifier.

Table S4. Clinical characteristics of the obese non-diabetic patients who underwent liver biopsy at the Antwerp University Hospital (N = 155).[9]

	mean ± SD
Gender (% male)	35.5
Age (years)	43.2 ± 12.9
BMI (kg/m2)	39.9 ± 5.6
Plasma Cholesterol (mg/dL)	203.6 ± 41.7
HDL-C (mg/dL)	47.5 ± 14
Plasma TG (mg/dL)	164.9 ± 86
LDL-C (mg/dL, calculated)	123.6 ± 37
Fasting Glucose (mg/dL)	86.1 ± 13.8
Fasting Insulin (µU/mL)	20.1 ± 18.3
HbA1c (%)	5.6 ± 0.6
HOMA-IR	4.5 ± 5.4
ASAT (U/L)	25.2 ± 14.7
ALAT (U/L)	40.4 ± 29.7
Alkaline Phosphatase (U/L)	78.1 ± 20.6
γGT (U/L)	50 ± 38.4

Table S5. Correlations between the expression of spliceosome genes, intron 3 (IVS3), or full length *LDLR* in the livers of obese non-diabetic patients (n=155)[9].

Gene	IVS3			Full length LDLR		
	Spearman correlation coefficient	Unadjusted p value	Adjusted p value	Spearman correlation coefficient	Unadjusted p value	Adjusted p value
SF3A1	0.01	$9.0 * 10^{-1}$	1.0	0.13	$1.1 * 10^{-1}$	1.0
SF3A2	-0.21	$8.9 * 10^{-3}$	$9.8 * 10^{-2}$	-0.085	$3.0 * 10^{-1}$	1.0
SF3B1	0.26	$1.3 * 10^{-3}$	$1.4 * 10^{-2}$	0.13	$9.9 * 10^{-2}$	1.0
SF3B2	0.066	$4.1 * 10^{-1}$	1.0	0.024	$7.6 * 10^{-1}$	1.0
SF3B4	0.065	$4.2 * 10^{-1}$	1.0	0.029	$7.2 * 10^{-1}$	1.0
SF3B5	0.067	$4.1 * 10^{-1}$	1.0	0.1	$2.0 * 10^{-1}$	1.0
SF3B6	0.058	$4.7 * 10^{-1}$	1.0	0.061	$4.5 * 10^{-1}$	1.0
RBM22	-0.031	$7.1 * 10^{-1}$	1.0	-0.0012	$9.9 * 10^{-1}$	1.0
RBM25	0.14	$8.4 * 10^{-2}$	1.0	-0.018	$8.2 * 10^{-1}$	1.0
ISY1	0.12	$1.3 * 10^{-1}$	1.0	0.086	$2.9 * 10^{-1}$	1.0
AQR	0.13	$1.2 * 10^{-1}$	1.0	-0.044	$5.9 * 10^{-1}$	1.0

Coefficients of correlation were calculated according to Spearman. Adjustment of p values for multiple testing was done according to Bonferroni correction.

.

Table S6: Correlations of Total and Lipoprotein Cholesterol levels with the expression of LDLR transcripts in the liver of non-diabetic obese patients

	probeID	total cholesterol	HDL cholesterol	LDL cholesterol	non-HDL cholesterol
5'UTR	16858387	-0.050	0.062	-0.092	-0.079
Exon1	16858388	-0.034	-0.047	-0.047	-0.030
Exon2	16858390	0.15	-0.0060	0.090	0.13
Exon2	16858391	0.094	-0.000032	0.034	0.059
Intron2	16858392	0.034	-0.055	0.022	0.018
Intron3	16858394	0.11	0.013	0.061	0.096
Exon4	16858395	0.023	-0.018	-0.021	0.029
Exon4	16858396	0.10	-0.070	0.065	0.10
Intron4	16858397	0.062	0.056	0.011	0.0082
Exon5	16858398	0.081	-0.042	0.033	0.077
Exon6	16858399	0.11	-0.11	0.12	0.16
Exon7	16858400	0.013	0.018	-0.019	0.00027
Exon8	16858401	-0.038	-0.032	-0.049	-0.035
Exon9	16858402	0.077	-0.062	0.092	0.084
Exon10	16858403	0.057	0.0017	0.019	0.031
Exon11	16858404	0.013	0.030	-0.029	-0.0092
Exon12	16858405	0.072	-0.032	0.026	0.062
Exon13	16858406	0.058	0.075	0.033	0.023
Exon13	16858407	0.16	0.11	0.061	0.083
Exon15	16858409	0.22	0.037	0.13	0.18
Intron15	16858410	0.067	0.063	0.0088	0.038
Exon16	16858411	0.034	0.059	-0.056	-0.010
Exon17	16858413	0.084	-0.0038	0.048	0.063
3´UTR	16858415	0.078	0.034	0.095	0.069
3´UTR	16858416	0.10	0.042	0.067	0.062

Data measured at baseline in the cohort described in Supplementary Table IV (n=155 patients)[9]. $\log_2$ transformed intensities of probes depicted in figure 5D were correlated with plasma lipid levels by Spearman. None of the correlations is statistically significant after adjustment for multiple testing with the Bonferroni correction (adjusted p value threshold $5*10^{-4}$.).

Table S7. Association between variants in spliceosome hit genes and multiple biochemical phenotypes in 40,468 UK Biobank exomes[11].

	Gene	LDL-C	ApoB	TG	HDL-C	ApoA	Chol.	Lp(a)	Glc	HbA1c
All Ethnicities coding-based model	*AQR*	0.32	0.45	0.59	0.18	0.35	0.17	0.71	0.29	0.73
	ISY1	0.87	0.67	0.64	0.16	0.17	0.69	0.93	0.42	0.2
	RBM25	0.22	0.31	0.59	0.72	0.81	0.3	0.74	0.39	0.061
	SF3A1	0.69	0.55	**0.007**	0.28	0.97	0.85	0.95	0.62	0.079
	SF3A2	0.66	0.34	0.86	0.1	0.089	0.94	0.18	0.11	**0.028**
	SF3B1	0.092	0.09	0.28	0.68	0.75	**0.043**	0.76	0.81	0.16
	SF3B2	0.66	0.52	0.54	0.49	0.36	0.9	0.7	0.62	0.41
	SF3B4	0.19	0.3	0.41	0.42	0.7	0.29	0.36	0.28	0.99
	SF3B5	0.77	0.51	0.93	0.19	0.089	0.77	0.88	0.25	0.23
	SF3B6	0.8	0.81	0.82	0.66	0.73	0.94	0.89	0.73	0.77
Eur Ethnicity coding-based model	*AQR*	0.73	0.78	0.69	0.47	0.62	0.6	0.65	0.19	0.88
	ISY1	0.93	0.47	0.43	0.22	0.21	0.94	0.72	0.41	0.29
	RBM25	0.28	0.4	0.81	0.97	0.78	0.35	0.52	0.51	0.12
	SF3A1	0.76	0.92	**0.039**	0.93	0.37	0.27	0.72	0.57	0.12
	SF3A2	0.77	0.6	0.65	**0.044**	0.063	0.74	0.51	0.59	0.081
	SF3B1	0.074	0.1	0.27	0.42	0.41	**0.032**	0.74	0.87	0.1
	SF3B2	0.49	0.38	0.57	0.91	1	0.56	0.76	0.47	0.056
	SF3B4	0.42	0.65	0.62	0.85	0.84	0.6	0.93	0.46	0.3
	SF3B5	0.88	0.8	0.7	0.2	0.23	0.77	0.95	0.07	0.12
	SF3B6	0.98	0.93	0.75	0.9	0.82	0.93	0.77	0.2	0.67
All Ethnicities LOF-based model	*AQR*	0.76	0.74	0.76	0.54	0.68	0.81	0.59	0.34	0.97
	ISY1	0.78	0.9	0.42	0.8	0.54	0.82	0.55	0.56	0.49
	RBM25	0.36	0.24	0.54	0.19	0.12	0.54	0.44	0.97	0.47
	SF3A1	0.98	0.94	0.5	0.83	0.66	0.88	1	0.44	0.98
	SF3A2	0.76	0.43	0.32	0.09	0.11	0.8	0.48	0.43	**0.037**
	SF3B2	0.47	0.27	0.64	0.94	0.9	0.67	0.37	0.27	0.49
	SF3B4	0.96	0.96	0.11	0.55	0.62	1	0.38	0.28	**0.008**
	SF3B5	0.4	0.16	0.78	0.14	0.065	0.58	0.86	0.24	0.32
	SF3B6	0.68	0.56	0.76	0.75	0.97	0.87	0.93	0.97	0.97

Table S7 (continued). Association between variants in spliceosome hit genes and multiple biochemical phenotypes in 40,468 UK Biobank exomes[11].

	Gene	LDL-C	ApoB	TG	HDL-C	ApoA	Chol.	Lp(a)	Glc	HbA1c
Eur Ethni-city LOF-based model	*AQR*	0.92	0.86	0.77	0.5	0.67	0.97	0.36	0.34	0.97
	ISY1	0.79	0.87	0.3	0.75	0.92	0.9	0.65	0.52	0.15
	RBM25	0.29	0.15	0.63	0.18	0.072	0.5	0.24	0.53	0.32
	SF3A1	0.96	0.96	0.56	0.89	0.67	0.94	1	0.45	0.88
	SF3A2	0.77	0.7	0.79	0.061	0.12	0.78	0.94	0.84	0.25
	SF3B2	0.34	0.22	0.27	0.79	0.85	0.52	0.63	0.45	0.23
	SF3B5	0.4	0.26	0.3	0.16	0.2	0.52	1	0.075	0.11
	SF3B6	0.83	0.76	0.71	0.92	0.84	0.83	0.79	0.27	0.48

No association was significant, neither at the genome-wide level (p value threshold $3.13*10^{-6}$) nor after correcting the p value for limited hypothesis testing (p value threshold 0.004545). Data are expressed as p values. Associations with p value below 0.05 are highlighted in bold. Non-standard abbreviations: Chol.: Total cholesterol; Glc: Glucose

Table S8. Gene-based constraint information from the gnomAD database for the spliceosomal hit genes.

Gene	pLI
SF3A1	0.99
SF3A2	0.88
SF3B1	1
SF3B2	1
SF3B4	0.99
SF3B5	0.58
SF3B6	0.59
RBM22	1
RBM25	1
ISY1	1
AQR	1
Average	0.91
SD	0.17

pLI = probability of being loss-of-function intolerant. pLI is an estimate of deleteriousness based on variant frequencies within that gene used in the GnomAD database. Metrics to measure a transcript's intolerance to variation by comparing the observed number of variants in the gnomAD dataset with the expected number of variants. Transcripts that are significantly depleted of their expected variation are considered constrained, or intolerant, of such variation. The closer pLI is to 1, the more intolerant of protein variants the transcript appears to be. pLI $\geq$ 0.9 is considered as an indication of extreme intolerance. For more details see supplement of reference[12] and https://gnomad.broadinstitute.org/).

Table S9. Meta analysis of associations between the rs 17570658 SNP of *RBM25* with LDL cholesterol

Dataset	Sample size	Z Score	p-value
UK Biobank Mendelian Trait GWAS	333541	-4.702	$2.6 * 10^{-6}$
Hoorn DCS2018	3414	-2.636	$8.4 * 10^{-3}$
GoDarts Illumina Infinium GWAS	1884	-1.282	$2.0 * 10^{-1}$
GLGC GWAS	84987	1.072	$2.8 * 10^{-1}$
Hoorn DCS2019	1997	-0.974	$3.3 * 10^{-1}$
Extend GWAS	7159	-0.697	$4.9 * 10^{-1}$
GoDarts Illumina Human OMNI Express	2902	-0.1	$9.2 * 10^{-1}$
Copenhagen City Heart and General Population Studies	19653	-0.722	$4.7 * 10^{-1}$
All together	**455537**	**-4.181**	**P = 2.9 * 10^{-5}**

All data except from Copenhagen City Heart and General Population Studies[13] are from the CardioVascular Disease Knowledge Portal (https://cvd.hugeamp.org/variant.html?variant=rs17570658) and were reanalyzed according to METAL[14].

Table S10. *RBM25* gene variants identified in 71 FH patients without any mutation in the three canonical FH genes.

rsID	hg 19 Chr:pos	cDNA	AA	GT	MAF	PPH2	SIFT	MT
NA	14:73554780	c.454A>T	p.I152F	het	0	PSD	D	DC
NA	14:73572776	c.1364C>A	p.A455D	het	0	PD	D	DC
rs1167173761	14:73538399	c.50T>C	p.L17P	het	$9*10^{-6}$	PD	D	DC

The overall p value for a gene burden test of rare variants (MAF<0.0001) in RBM25 identified in 71 FH mutation negative patients[15] in comparison to the gnomAD data of 56,352 individuals was p= 0.001. The three RBM25 variants listed in the table were identified in 3 FH probands and were unique to those individuals. Coordinates refer to the canonical ENST00000261973 transcript. AA: amino acid; GT: genotype; het: heterozygote; MAF: minor allele frequency in the GnomAD database; PPH2: PolyPhen 2; SIFT: Sorting Intolerant From Tolerant ;MT: Mutation Taster; PSD: Possibly Damaging; PD: Probably Damaging; D: Damaging; DC: Disease Causing

Table S11: PCR primersequences for all primer couples used in this study.

Experiment/primer	5'-3' Sequence
LDLRret fragment cloning	
F	ATGGGGCCCTGGGGCTGG
R	TCAGATAGGCTCAATAGCAAAGGCA
Short pSPL3 minigene cloning	
F	CTAGCGAATTCGCAAAGACAGGATTGGCAAGG
R	CTAGCGGATCCTGGTATGAGCCCCCAAGAGA
Long pSPL3 minigene cloning	
F	GCTAGCGAATTCTGCAAAGACAGGATTGGCAAG
R	CTAGCGGATCCTGGAAATCCACTTCGGCACC
Determination of siRNA knockdown efficiency in Huh-7	
SF3A1 – F	TGTTACCGAGTGGAATGGGC
SF3A1 – R	GATCTGAGCATAGGCCACCC
SF3A2 – F	TCG ACA TCA ACA AGG ACC CG
SF3A2 – R	GCT TCT TCC CCT GCG TAT GT
SF3B1 – F	AGATCGCCAAGACTCACGAAG
SF3B1 – R	ACCTGTAGAATCGAGGCCCA
SF3B2 – F	CTATGGCCCACCCACCAAAT
SF3B2 – R	CGAATGATCTCCCTGCTGCT
SF3B4 – F	TCAGGATGCCACTGTGTACG
SF3B4 – R	TCCTTTGGCATGTGGGTGTT
SF3B5 – F	CCGCTACACCATCCATAGCC
SF3B5 – R	GCCCATGTAGGAGCAGTACG
SF3B6 – F	GGC GAA CAT TCG ACT TCC AC
SF3B6 – R	GGT GTG TTC CCC ACT CTG AT
RBM22 – F	TCGTGACGCAGGATTGTCTT
RBM22 – R	TAGATGTGGCTTTCCCCAGC
RBM25 – F	AGCCAGAATCTACCCTCCGT
RBM25 – R	TCTGGCCTTGCATTCCCATT
ISY1 – F	GGCCCGAAATGCAGAAAAGG
ISY1 – R	GGCCAGAAAGGGTCTTCGTT

Table S11 (continued): PCR primersequences for all primer couples used in this study.

Experiment/primer	5'-3' Sequence
AQR – F	GGCGGCATTAGCTGAAACTG
AQR – R	CAGCTGTAAGCCCATCCACA
LDLR – F	AAG GAC ACA GCA CAC AAC CA
LDLR – R	CAT TTC CTC TGC CAG CAA CG
GAPDH – F	CCCATGTTCGTCATGGGTGT
GAPDH – R	TGGTCATGAGTCCTTCCACGATA
LDLR expression and IVS3 retention in human liver and Huh-7 cells (from[5])	
LDLR canonical transcript - F	GACAACGGCTCAGACGAGCA
LDLR canonical transcript - R	CCACAGGTGAGCACCGGGCA
IVS3 retention – F	GTGATGGTGGTCTCGGCCCA
IVS3 retention – R	GGACCACAGGTGAGCACCGG

IVS3: intron 3. F: forward primer, R: reverse primer

Table S12: gene boundaries for the annotation of the UK Biobank GWAS data.

Gene	chr	Start	End
AQR	15	35148551	35261995
ISY1	3	128846258	128880073
RBM22	5	150070351	150080669
RBM25	14	73525220	73588076
SF3A1	22	30727976	30752936
SF3A2	19	2236815	2248678
SF3B1	2	198256697	198299817
SF3B2	11	65819815	65836382
SF3B4	1	149895208	149900144
SF3B5	6	144416017	144416754
SF3B6	2	24290453	24299314

Coordinates refer to the GRCh37/hg19 build

4. Major Resources Tables

Antibodies

Target antigen	Vendor or Source	Catalog #	Working concentration (µg/ml)	Lot #	Persistent ID / URL
LDLR	Abcam,	Ab52818	0.67 (WB)	GR3253668-2	**AB881213**
RBM25	Abcam	Ab72237	0.2 (WB)	GR3364959-1	**AB1270216**
Polyclonal Goat anti-Rabbit HRP Conjugated Immunoglobulins	Dako, Agilent Pathology Solutions,	P0448	0.05 (WB)	20061231	**AB2617138**
Polyclonal Rabbit anti-Mouse HRP conjugated Immunoglobullins	Dako, Agilent Pathology Solutions	P0260	0.26 (WB)	20039216	**AB2636929**
Polyclonal Rabbit Anti-Goat HRP conjugated Immunoglobulins	Dako, Agilent Pathology Solutions	P0449	0.1 (WB)	00062104	**AB2617143**
HRP-conjugated anti-HA antibody	Sigma Aldrich	H6533	2 (WB)	NA	**AB439705**
TBP	Abcam,	Ab51841	1 (WB)	GR103882-2	**AB945758**
Beta actin	Santa Cruz Biotechnology	SC-1616	0.1 ug/ml	NA	**AB630836**
LDLR	Santa Cruz Biotechnology	sc- 18823	2 (flow cytometry)	NA	**AB627881**
LDLR	PROGEN Biotechnik GmbH	61087	2 (flow cytometry)	207100-01	**AB1542236**
Isotype control antibody	Santa Cruz Biotechnology)	sc-3879	2 (flow cytometry)	L0816	**AB737262**
chicken anti-Mouse IgG (H+L) Cross-Adsorbed AlexaFluor 488-conjugated Secondary Antibody	Thermo Fisher Scientific	A-21200	4 (flow cytometry)	NA	**AB2535786**
Goat anti-Mouse IgG (H+L) Cross-Adsorbed AlexaFluor 647-conjugated Secondary Antibody	Thermo Fisher Scientific	A-21236	4 (flow cytometry)	1915660	**AB2535805**

DNA/cDNA Clones

Clone Name	Sequence	Source / Repository	Persistent ID / URL
LDLR ret fragment	ENST00000557958.1: nt 87-437	Cloned in house	NA
HA tagged LDLR fragment	N-terminally HA-tagged version of ENST00000557958.1: nt 87-437	Invitrogen GeneArt Strings DNA Fragments (Thermo Fisher Scientific)	NA
short LDLR minigene	hg38 chr19:11,102,285-11,102,921	Cloned in house	NA
long LDLR minigene	hg38 chr19:11,102,283-11,105,702	Cloned in house	NA
Wild type RBM25	NM_021239.3:188-2719	proteogenix	NA
RBM25 p.L17P	NM_021239.3:188-2719 (c.50T>C)	proteogenix	NA
RBM25 p.I152F	NM_021239.3:188-2719 (c.454A>T)	proteogenix	NA
RBM25 p.A455D	NM_021239.3:188-2719 (c.1364C>A)	proteogenix	NA

Cultured Cells

Name	Vendor or Source	Catalog #	Sex (F, M, or unknown)	Persistent ID / URL
Huh-7	Japanese Collection or Research Bioresources Cell Bank, JCRB Cell Bank, Osaka, Japan	JCRB0403	M	**CVCL_0336**
HepG2	American Type Culture Collection, ATCC, Manassas, VA, USA	HB-8065	M	**CVCL_0027**
HEK293T	American Type Culture Collection, ATCC, Manassas, VA, USA	CRL-3216	F	**CVCL_0063**

Data & Code Availability

Description	Source / Repository	Persistent ID / URL
Homo Sapiens reference genome	Data Sciences Platform at the Broad Institute/ build GRCh38 and build GRCh37/h19	https://gatk.broadinstitute.org/hc/en-us/articles/360035890951-Human-genome-reference-builds-GRCh38-or-hg38-b37-hg19 and https://gatk.broadinstitute.org/hc/en-us/articles/360035890711-GRCh37-hg19-b37-humanG1Kv37-Human-Reference-Discrepancies
UCSC Genome Browser Variant Annotation Integrator	Variant Annotation Integrator	https://genome.ucsc.edu/cgi-bin/hgVai
U2 branchpoint prediction algorithm	SVM-BP-finder	http://regulatorygenomics.upf.edu/Software/SVM_BP/
Expression of LDLR transcripts in healthy human liver	Gene Expression Omnibus,	GSE126848/ https://www.ncbi.nlm.nih.gov/geo/query/acc.cgi?acc=GSE126848L
SNP data from UK Biobank	UK Biobank	http://www.nealelab.is/uk-biobank
Meta analysis of rs 17570658	CardioVascular Disease Knowledge Portal	(https://cvd.hugeamp.org/variant.html?variant=rs17570658)
exome variants of UK Biobank	Helix Research and UK Biobank	server s3://helix-researchpublic/ukbb_exome_analysis_results/V1.3
UK10K	Patient specific data not shared. Summary data previously published in DOI: 10.1136/jmedgenet-2014-102405	https://www.uk10k.org/data_access.html
Expression analysis of spliceosome genes in various tissues	Genotype-Tissue Expression (GTEx) project	https://gtexportal.org/home

Data & Code Availability (continued)

Description	Source / Repository	Persistent ID / URL
gnomAD Databank	genome aggregation database	https://gnomad.broadinstitute.org/
RNA sequencing of Huh7 cells treated with siRNAs against spliceosome genes or scrambled siRNA	European Nucleotide Archive	https://www.ebi.ac.uk/ena/browser/support: accession codes PRJEB46898 and PRJEB46899

siRNAs and Transfection reagents

Description	Source / Repository	Catalog #	Persistent ID / URL
Lipofectamine™ RNAiMAX Transfection Reagent	Thermo Fisher Scientific	13778150	https://www.thermofisher.com/order/catalog/product/13778150#/13778150
Lipofectamine™ 2000 Transfection Reagent	Thermo Fisher Scientific	11668019	https://www.thermofisher.com/order/catalog/product/11668019#/11668019
Lipofectamine™ 3000 Transfection Reagent	Thermo Fisher Scientific	L3000015	https://www.thermofisher.com/order/catalog/product/L3000015#/L3000015
The Ambion Silencer Select Human Genome siRNA library V4	Thermo Fisher Scientific	4397926	https://www.thermofisher.com/order/catalog/product/4397926?SID=srch-hj-4397926#/4397926?SID=srch-hj-4397926
Ambion Silencer Select anti-*PLK1*	Thermo Fisher Scientific	assay ID s448, cat. 4390824	https://www.thermofisher.com/order/genome-database/details/sirna/s448?CID=&ICID=&subtype=
Ambion Silencer Select anti-*LDLR*	Thermo Fisher Scientific	assay ID s4, cat. No. 4392420	https://www.thermofisher.com/order/genome-database/details/sirna/s4?CID=&ICID=&subtype=sirna_silencer_select
Silencer™ Select Negative Control No. 1 siRNA	Thermo Fisher Scientific	4390843	https://www.thermofisher.com/order/catalog/product/4390843#/4390843

siRNAs and Transfection reagents (continued)

Description	Source / Repository	Catalog #	Persistent ID / URL
SF3A1	Dharmacon	L-016051-00-0005	https://horizondiscovery.com/en/gene-modulation/knockdown/sirna/products/on-targetplus-sirna-reagents?nodeid=entrezgene-10291
SF3A2	Dharmacon	L-018282-02-0005	https://horizondiscovery.com/en/gene-modulation/knockdown/sirna/products/on-targetplus-sirna-reagents?nodeid=entrezgene-8175
SF3B1	Dharmacon	L-020061-01-0005	https://horizondiscovery.com/en/gene-modulation/knockdown/sirna/products/on-targetplus-sirna-reagents?nodeid=entrezgene-23451
SF3B2	Dharmacon	L-026599-01-0005	https://horizondiscovery.com/en/gene-modulation/knockdown/sirna/products/on-targetplus-sirna-reagents?nodeid=entrezgene-10992
SF3B4	Dharmacon	L-017190-00-0005	https://horizondiscovery.com/en/gene-modulation/knockdown/sirna/products/on-targetplus-sirna-reagents?nodeid=entrezgene-10262
SF3B5	Dharmacon	L-014706-02-0005	https://horizondiscovery.com/en/gene-modulation/knockdown/sirna/products/on-targetplus-sirna-reagents?nodeid=entrezgene-83443
SF3B6	Dharmacon	L-020260-02-0005	https://horizondiscovery.com/en/gene-modulation/knockdown/sirna/products/on-targetplus-sirna-reagents?nodeid=entrezgene-51639
RBM22	Dharmacon	L-021186-01-0005	https://horizondiscovery.com/en/gene-modulation/knockdown/sirna/products/on-targetplus-sirna-reagents?nodeid=entrezgene-55696
RBM25	Dharmacon	L-021976-00-0005	https://horizondiscovery.com/en/gene-modulation/knockdown/sirna/products/on-targetplus-sirna-reagents?nodeid=entrezgene-58517

siRNAs and Transfection reagents (continued)

ISY1	Dharmacon	L-013894-01-0005	https://horizondiscovery.com/en/gene-modulation/knockdown/sirna/products/on-targetplus-sirna-reagents?nodeid=entrezgene-57461
AQR	Dharmacon	L-022214-01-0005	https://horizondiscovery.com/en/gene-modulation/knockdown/sirna/products/on-targetplus-sirna-reagents?nodeid=entrezgene-9716
Non-targeting control pool	Dharmacon	D-001810-10-05	https://horizondiscovery.com/en/gene-modulation/knockdown/controls/products/on-targetplus-non-targeting-control-pool?catalognumber=D-001810-10-05
MISSION® predesigned siRNA against RBM25	Sigma-Aldrich	SASI_Hs02_00354878	https://www.sigmaaldrich.com/CH/en/semi-configurators/sirna?activeLink=selectAssays
MISSION® siRNA Universal Negative Control #2	Sigma-Aldrich	SIC002	https://www.sigmaaldrich.com/CH/en/product/sigma/sic002